# Polytopic membrane protein folding at L17 in the ribosome tunnel initiates cyclical changes at the translocon

Pen-Jen Lin,[1] Candice G. Jongsma,[2] Martin R. Pool,[4] and Arthur E. Johnson[1,2,3]

[1]Department of Molecular and Cellular Medicine, Texas A&M Health Science Center, and [2]Department of Chemistry and [3]Department of Biochemistry and Biophysics, Texas A&M University, College Station, TX 77843
[4]Faculty of Life Sciences, University of Manchester, Manchester M13 9PT, England, UK

Multi-spanning membrane protein loops are directed alternately into the cytosol or ER lumen during cotranslational integration. Nascent chain exposure is switched after a newly synthesized transmembrane segment (TMS) enters the ribosomal tunnel. FRET measurements revealed that each TMS is initially extended, but folds into a compact conformation after moving 6–7 residues from the peptidyltransferase center, irrespective of loop size. The ribosome-induced folding of each TMS coincided with its photocrosslinking to ribosomal protein L17 and an inversion of compartmental exposure. This correlation indicates that successive TMSs fold and bind at a specific ribosomal tunnel site that includes L17, thereby triggering structural rearrangements of multiple components in and on both sides of the ER membrane, most likely via TMS-dependent L17 and/or rRNA conformational changes transmitted to the surface. Thus, cyclical changes at the membrane during integration are initiated by TMS folding, even though nascent chain conformation and location vary dynamically in the ribosome tunnel. Nascent chains therefore control their own trafficking.

## Introduction

In eukaryotes, the cotranslational integration of a multi-spanning polytopic membrane protein (PMP) into the endoplasmic reticulum (ER) membrane is accomplished by two molecular machines that are coupled together to form the ribosome–translocon complex (RTC; Alder and Johnson, 2004; Rapoport, 2007; Johnson, 2009; Skach, 2009). Proper threading of a PMP into the ER membrane is complex, requiring accurate delivery of successive loops to the cytosol and ER lumen while simultaneously maintaining membrane integrity to avoid unregulated lumenal Ca$^{2+}$ leakage into the cytosol and its deleterious effect on the cell. In addition to the RTC, proteins such as RAMP4 (Pool, 2009), importin α-16 (Saksena et al., 2006), and others are intimately involved. Their actions must be coordinated with those of the RTC to ensure that one end of the aqueous translocon pore is sealed at all times: the lumenal end by the action of, among others, BiP and a J-domain–containing ER membrane protein (Hamman et al., 1998; Haigh and Johnson, 2002; Alder et al., 2005), and the cytosolic end by an ion-tight ribosome–translocon junction (Crowley et al., 1994; Hamman et al., 1997; Liao et al., 1997; Lin et al., 2011) that also involves TRAM (Hegde et al., 1998), calmodulin (Erdmann et al., 2011), an unknown protein (Devaraneni et al., 2011), and possibly others. The need to synchronize molecular interactions and the resulting structural changes in the membrane and two cellular compartments introduces additional complexities into the mechanically intricate integration process.

During PMP integration, the entry of each TMS into the ribosomal tunnel (in this paper, "tunnel" = ribosome tunnel, and "pore" = translocon pore) triggers major changes in the conformation and composition of the extended RTC complex that includes BiP, RAMP4, and others in and on both sides of the membrane (see accompanying paper, Lin et al., 2011).

The Rockefeller University Press $30.00
J. Cell Biol. Vol. 195 No. 1 55–70
www.jcb.org/cgi/doi/10.1083/jcb.201103118

JCB 55

These changes cycle between two different states that alternately expose the nascent PMP chain to the cytosol or to the lumen. Each inversion of RTC structure is initiated when the triggering TMS is still relatively close to the peptidyltransferase center (PTC; Lin et al., 2011). The ribosome must therefore scan the nascent chain as it passes through the tunnel to detect the presence of a TMS, and a successful TMS identification must involve a direct and specific interaction between the ribosome and the nascent chain.

A nascent chain–ribosome interaction inside the tunnel with functional ramifications was identified by Liao et al. (1997), who showed that ribosomal recognition of the TMS in a single-spanning membrane protein (SSMP) elicited structural rearrangements on both sides of the membrane. The authors proposed that TMS recognition involved its folding into an α-helix inside the ribosome tunnel (Liao et al., 1997), a prediction later verified by fluorescence resonance energy transfer (FRET) data (Woolhead et al., 2004). TMS folding in the tunnel was also detected for the third TMS (TMS3) of aquaporin using photocrosslinking (Daniel et al., 2008) and the N termini of five of the six TMSs in Kv1.3, a voltage-gated K+ channel, folded near the tunnel exit (Lu and Deutsch, 2005b; Tu and Deutsch, 2010). On the other hand, TMS folding was not detected in bacterial RNCs that were not bound to the membrane (Houben et al., 2005). Photocrosslinking data in the eukaryotic system also showed that the newly folded nascent SSMP TMS was adjacent to proteins in the eukaryotic ribosome tunnel (Liao et al., 1997), and ribosomal protein L17 was later identified as part of a TMS-sensitive signaling pathway to the membrane (Woolhead et al., 2004). This last prediction was verified when chemical cross-linking data revealed that the appearance of a nascent chain SSMP TMS in the tunnel caused a structural rearrangement at the RTC (Pool, 2009).

Other nascent chain sequences interact with ribosomal components in the tunnel to control translation (Ito et al., 2010; Cruz-Vera et al., 2011). Four such nascent proteins have so far been shown to adopt specific conformations within the ribosome tunnel, as shown by FRET (Woolhead et al., 2006) and cryoelectron microscopy (cryoEM; Seidelt et al., 2009; Bhushan et al., 2010b, 2011). In addition, other nascent chain sequences have been shown to alter ribosome conformation from inside the tunnel and thereby increase ribosome-nascent chain complex (RNC) affinity for cytosolic factors: signal-anchor sequences inside the tunnel increased RNC affinity for the signal recognition particle (SRP; Berndt et al., 2009), whereas tail-anchored membrane protein TMSs recruited Bat3 complexes to RNCs (Mariappan et al., 2010). In each of the above cases, a specific nascent chain–ribosome interaction inside the tunnel triggered a single transition that regulated translation (on to off), targeting (low affinity SRP and Bat3 complex binding to high), or integration (SSMP movement into the cytosol instead of the lumen).

During PMP integration, each TMS that entered the ribosome tunnel initiated a change in RTC structure (Lin et al., 2011). Moreover, successive TMSs caused the RTC structure to cycle between two structural states that expose the ribosome tunnel to either the lumen or the cytosol. Because exchanging the order of TMSs in the nascent chain did not alter the pattern of lumenal or cytosolic nascent chain exposure (Lin et al., 2011), how does a single nascent chain structural feature, a TMS, elicit two different outcomes? As a first step in understanding this cyclical process, we have examined nascent chain interactions in the ribosome tunnel for periodicity in two RTC-dependent structural properties, ribosome-induced TMS conformation and L17 proximity. Does each PMP TMS fold into a helix in the ribosome tunnel? Or do alternate TMSs fold (e.g., TMS1 and TMS3)? Does each TMS fold at the same ribosome tunnel location? Is every PMP TMS exposed to L17, or are only alternate TMSs adjacent to L17?

## Results

### Approach

Nascent protein folding was detected by incorporating two fluorescent dyes into the same polypeptide and monitoring their separation by FRET. If one dye (the donor) is excited by absorbing a photon, its excitation energy can be transferred to a second chromophore (the acceptor) without the emission of a photon. The efficiency of this energy transfer, E, is highly dependent on R, the distance between donor and acceptor dyes: $E = R_0^6/(R^6 + R_0^6)$, where $R_0$ is the dye separation when E is 50%. The extent of TMS folding was examined by placing dyes 24 residues apart at opposite ends of a TMS (Fig. 1 A). If the nascent chain were fully extended, the dyes would be separated by ∼80 Å and E would be ∼4% for the donor–acceptor pair used here. But if the TMS folded into a more compact structure, the dye separation would decrease substantially and E would increase.

The most accurate way to determine E is to quantify the acceptor-dependent decrease in donor emission intensity or lifetime. But proper controls must be done because a significant background signal is observed even with the best instruments due to the efficient light scattering of ribosome-bound ER microsomes. Four matched samples are prepared in parallel that differ only in the presence or absence of the donor and acceptor dyes, and they are designated D (donor-containing), DA (donor- and acceptor-containing), A (acceptor-containing) and B (blank sample with no donor or acceptor dyes). Subtraction of the B signal from that of D corrects for light scattering and background fluorescence, and yields the net donor intensity in the absence of acceptor. Subtraction of the A signal from that of DA corrects for background and scattering, as well as any signal due to direct excitation of the acceptor, and yields the net donor intensity in the presence of acceptor. The number of donor dyes in D and DA is determined using radioactivity, and the net donor intensities are normalized to the same number of donor dyes before calculating E. Because every nascent chain with a donor dye in the DA sample should also contain an acceptor dye, E is determined from the net emission intensities per donor dye of the D and DA samples.

Nascent chains constitute only ∼0.1% of the total protein in the samples used here. Thus, selective labeling of nascent chains can only be accomplished by incorporating the dyes into the nascent chain as it is being synthesized by the ribosome.
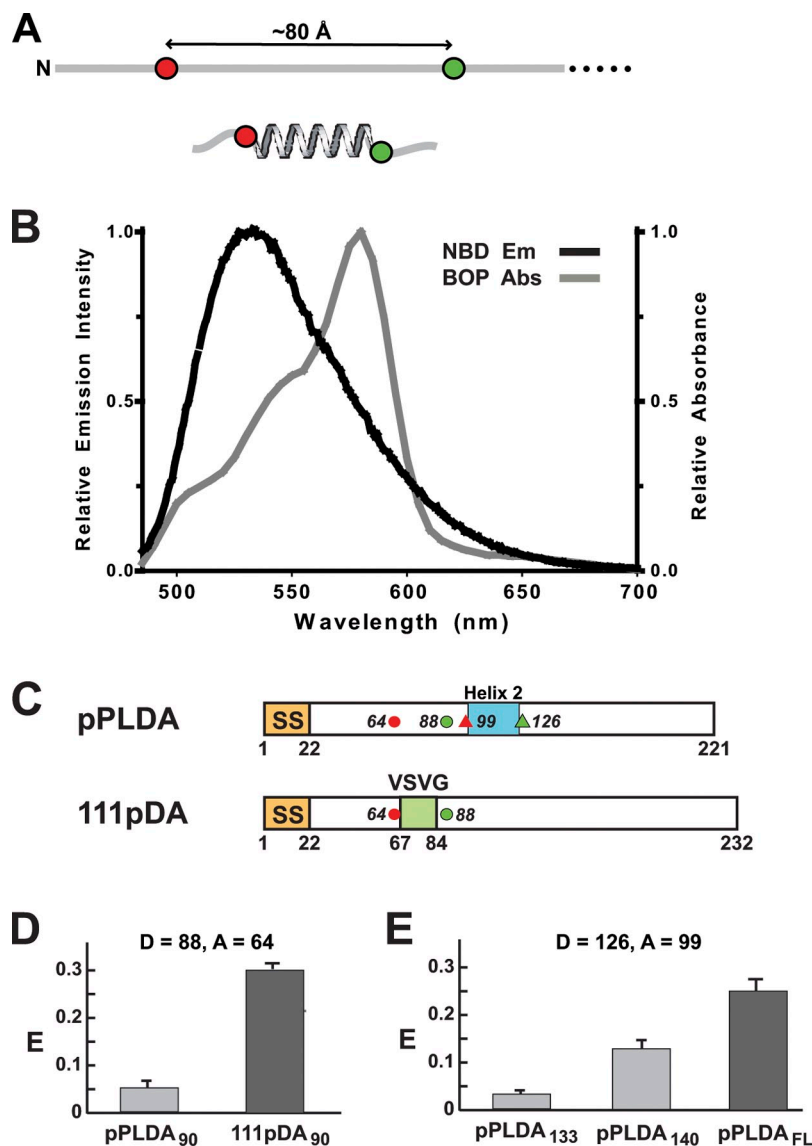
**Figure 1. NBD to BOP FRET.** (A) One acceptor dye (red) and one donor dye (green) are incorporated into the same nascent chain 24 residues apart (~80 Å when fully extended). If the nascent protein folds into an α-helix between the dyes, dye separation is greatly reduced. (B) Spectral overlap of donor NBD emission (black) and acceptor BOP absorbance (gray). (C) Topogenic sequence and dye locations are indicated in the primary structures of preprolactin (pPL) and an SSMP (111p): non-TMS helix 2 (blue); VSVG TMS (green); signal sequence (SS; orange); dyes as in A (in pPL, one placement shown with circles, the other with triangles). (D and E) Average FRET efficiencies ± SD obtained in three or more independent experiments for (D) $pPLDA_{90}$ and $111pDA_{90}$ RTCs with same probe locations, and (E) pPLDA RTCs with different nascent chain lengths and dyes flanking PL helix 2. FL = full-length; folded helices in black.

This approach requires modified aminoacyl-tRNAs (Johnson et al., 1976; Johnson, 2005a) that recognize a particular codon during in vitro translation, but incorporate an amino acid analogue with a fluorescent dye covalently attached to its side chain instead of the natural amino acid. In the DA sample, $N^\varepsilon$-6(7-nitrobenz-2-oxa-1,3-diazol-4-yl)aminohexanoyl-Lys-tRNA$^{Lys}$ ($\varepsilon$NBD-Lys-tRNA$^{Lys}$) incorporated an NBD donor dye at a lysine codon in the mRNA, whereas the amber suppressor $\varepsilon$BOP-Lys-tRNA$^{amb}$ incorporated a BODIPY 576/589 (BOP) acceptor dye at an amber stop codon. To avoid any complications in the control samples due to the charge on unmodified lysine, $N^\varepsilon$-acetyl-Lys-tRNA$^{amb}$ ($\varepsilon$Ac-Lys-tRNA$^{amb}$) replaced $\varepsilon$BOP-Lys-tRNA$^{amb}$ in the D and B translations, and $\varepsilon$Ac-Lys-tRNA$^{Lys}$ replaced $\varepsilon$NBD-Lys-tRNA$^{Lys}$ in A and B.

To ensure only one donor and one acceptor per nascent chain, mRNAs contained a single in-frame copy of each of those codons. Because $\varepsilon$NBD-Lys-tRNA$^{Lys}$ competes with endogeneous Lys-tRNA$^{Lys}$ for the Lys codon during translation and $\varepsilon$BOP-Lys-tRNA$^{amb}$ competes with termination factors for the amber codon, a fluorescent amino acid will not be incorporated at every Lys or amber codon. To avoid the possibility of nascent chains with a donor dye having no acceptor dye, it is absolutely essential that the amber codon precede the Lys codon in the mRNA. The reasons for this and other critical experimental design principles have been thoroughly explained in Woolhead et al. (2004) and are not repeated here. RTCs with PMP nascent chains of defined length were prepared by translating truncated mRNAs in vitro in the presence of SRP, ER microsomes, and the appropriate modified aa-tRNAs. The same PMPs and lengths were used here and in the accompanying paper (Lin et al., 2011) to facilitate data correlation, but the number, type, and location of probes varied.

## Choice of donor dye

BODIPY FL (BOF) was the donor dye in the original FRET studies (Woolhead et al., 2004, 2006). However, to reduce experimental uncertainty, we have here used NBD as the donor. $\varepsilon$NBD-Lys is incorporated into protein at the same rate and to the same extent as unmodified Lys (Crowley et al., 1993), the spectral overlap of NBD emission and BOP absorbance is
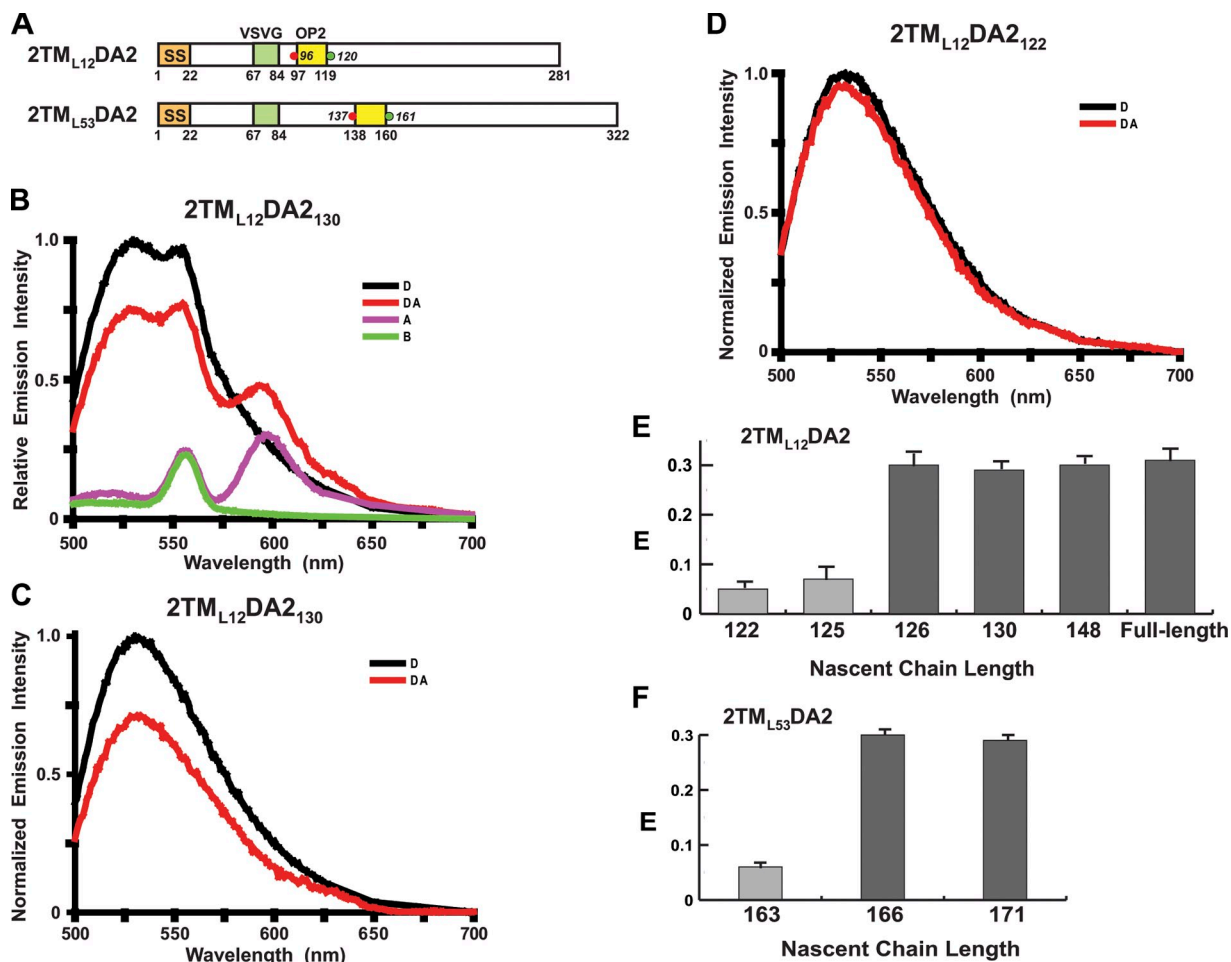
**Figure 2.** **FRET-detected TMS2 folding.** (A) Topogenic sequence and dye locations are depicted as in Fig. 1. TMS2 = opsin 2 (yellow). (B) Emission spectra of the $2TM_{L12}DA2_{130}$ D (black), DA (red), A (purple), and B (green) samples. NBD emission peaks at 530 nm, BOP emission peaks at 596 nm, and the water Raman peak is at 556 nm. (C and D) Net normalized donor emission spectra for the D (black) and DA (red) samples of (C) $2TM_{L12}DA2_{130}$ and (D) $2TM_{L12}DA2_{122}$. (E and F) Average E ($\pm$SD) values obtained in three or more independent experiments for (E) $2TM_{L12}DA2$ and (F) $2TM_{L53}DA2$ RTCs with different nascent chain lengths and folded (black) or unfolded (gray) TMSs.

excellent (Fig. 1 B), and the instruments used here can reproducibly quantify net NBD intensities in aqueous media at ∼1 nM. To directly compare NBD-BOP and BOF-BOP E values, RTCs were prepared with 90-residue nascent chains of the proteins examined in the original study, the secretory protein preprolactin (pPL) and the SSMP designated 111p (Fig. 1 C). NBD-BOP E values for the 24-residue nascent chain segments inside the ribosome tunnel were 6 ± 1% for $pPLDA_{90}$ and 29 ± 1% for $111pDA_{90}$ (Fig. 1 D), and the corresponding BOF-BOP E values were 10 ± 1% and 47 ± 5% (Woolhead et al., 2004). Thus, both donor–acceptor pairs showed that the nascent secretory protein segment was extended within the ribosome tunnel, whereas the nascent SSMP TMS folded into a compact structure inside the tunnel.

$R_0(2/3)$, the $R_0$ value assuming free rotation of the donor and acceptor dyes ($\kappa^2 = 2/3$), was determined experimentally to be 47 Å for the NBD-BOP pair and 57 Å for the BOF-BOP pair (Woolhead et al., 2004). Using these values and the above efficiencies, the average distance between the donor and acceptor dyes for the 111p TMS in the ribosome tunnel was found to be 55 ± 1 Å for the NBD-BOP pair and 58 ± 2 Å for the BOF-BOP pair.

Because the dye separations measured by the two pairs were indistinguishable when R was near $R_0$ (i.e., when FRET measurements are most sensitive to changes in the distance between the donor and acceptor), the two donor–acceptor pairs are spectroscopically equivalent.

## TMS2 folds in the ribosome tunnel

To determine whether the second TMS (TMS2) of a PMP folds as it moves through the tunnel, integration intermediates containing $2TM_{L12}DA2_{130}$ nascent chains were prepared (Fig. 2 A; 2TM is the number of TMSs in the PMP, L12 is the size of the loop between TMS1 and TMS2, 130 is the length of the nascent chain, and DA2 indicates that the donor and acceptor dyes flank TMS2). The emission spectra obtained for the D, DA, A, and B samples are shown in Fig. 2 B, and the net D and net DA spectra are shown in Fig. 2 C. Because the presence of the acceptor decreased donor emission intensity in this experiment (E = 30%), the dyes were close enough to exhibit substantial FRET. In contrast, little FRET was detected (E = 6% in this experiment) when RTCs with $2TM_{L12}DA2_{122}$ nascent chains were examined (Fig. 2 D). Because the fluorescence

Table I. **Fluorescence lifetimes of NBD at C terminus of TMS in various 2TM$_{L12}$K2 species[a]**

| NBD-labeled species | Membranes | Donor–PTC separation[b] | NBD location | $\tau_1$ | $f_1$[c] | $\tau_2$ | $f_2$[c] | $\chi^2$ | $< \tau >$[d] |
|---|---|---|---|---|---|---|---|---|---|
| | | | | *nsec* | | *nsec* | | | *nsec* |
| 2TM$_{L12}$DA2$_{122}$ | + | 2 | Tunnel | 2.8 ± 0.1 | 0.70 | 9.1 ± 0.3 | 0.30 | 3 | 4.7 ± 0.2 |
| 2TM$_{L12}$DA2$_{125}$ | + | 5 | Tunnel | 2.9 ± 0.2 | 0.68 | 9.6 ± 0.5 | 0.32 | 1 | 5.0 ± 0.3 |
| 2TM$_{L12}$DA2$_{126}$ | + | 6 | Tunnel | 2.5 ± 0.2 | 0.64 | 8.5 ± 0.3 | 0.36 | 3 | 4.7 ± 0.2 |
| 2TM$_{L12}$DA2$_{130}$ | + | 10 | Tunnel | 3.1 ± 0.1 | 0.76 | 10.1 ± 0.4 | 0.24 | 3 | 4.8 ± 0.2 |
| 2TM$_{L12}$DA2$_{FL}$[e] | + | − | Membrane | 3.0 ± 0.2 | 0.67 | 10.1 ± 0.4 | 0.33 | 2 | 5.3 ± 0.3 |
| 2TM$_{L12}$DA2$_{130}$[f] | − | 10 | Tunnel | 2.9 ± 0.2 | 0.71 | 9.9 ± 0.5 | 0.29 | 5 | 4.9 ± 0.3 |
| 2TM$_{L12}$DA2$_{180}$[f] | − | 60 | Solvent | 1.5 ± 0.1 | 0.77 | 8.3 ± 0.2 | 0.23 | 2 | 3.1 ± 0.1 |
| 2TM$_{L12}$DA2$_{130}$[g] | − | − | Solvent | 1.7 ± 0.1 | 0.88 | 8.8 ± 0.4 | 0.12 | 1 | 2.6 ± 0.1 |
| 2TM$_{L12}$DA2$_{130}$[h] | − | − | Solvent | 1.9 ± 0.1 | 0.98 | 7.4 ± 2.0 | 0.02 | 2 | 2.0 ± 0.1 |

[a]For each RTC, data from three or more independent experiments were combined and analyzed together as described in Materials and methods.

[b]Donor–PTC separation = nascent chain residues between the PTC and the εNBD-Lys at residue 120 in the nascent chain; in these experiments, no acceptor dye was present.

[c]Molar fraction

[d]Average lifetime calculated from molar fractions.

[e]Full-length 2TM$_{L12}$K2 proteins were translated, released from the translocon, and integrated into the ER membrane; note that the donor dye will be located in the membrane–lumen interface, not in the lipid core of the bilayer.

[f]RNC sample prepared without microsomes or SRP.

[g]RNC sample treated with puromycin, EDTA, and RNase to release the nascent chain from the ribosome into the solvent.

[h]RNC sample treated with puromycin, EDTA, and RNase to release the nascent chain from the ribosome; proteinase K was added to digest the nascent chain.

lifetimes and rotational rates of the donor dyes were nearly the same for 2TM$_{L12}$DA2$_{122}$ and 2TM$_{L12}$DA2$_{130}$ (Tables I and II), the large difference in E values for the two nascent chains did not result from changes in quantum yield or a $\kappa^2$ effect. Instead, the ΔE can only be explained by a substantial change in donor–acceptor separation. Thus, the TMS2 segment is, on average, almost fully extended after its synthesis, but it soon folds into a more compact conformation that brings the dyes closer together inside the ribosome tunnel.

When additional lengths of 2TM$_{L12}$DA2 were examined to determine exactly when TMS2 folded, the transition from unfolded to folded was found to be surprisingly abrupt. The addition of only a single amino acid to the end of a 125-residue nascent chain resulted in a dramatic increase in E, caused by TMS2 folding into a more compact conformation when its C terminus was 7 residues from the PTC (Fig. 2 E). This sharp transition strongly suggests that TMS folding is ribosome induced and occurs at a specific location within the ribosome tunnel. The only chemical differences between the 2TM$_{L12}$DA2$_{125}$ and 2TM$_{L12}$DA2$_{126}$ samples were nascent chains that differed in length by 1 residue and the truncated mRNAs that differed in length by three nucleotides. Thus, the change in E resulted solely from a change in TMS environment within the ribosome tunnel as 2TM$_{L12}$DA2 reached a length of 126 residues. The FRET-detected conformational change in the nascent chain was presumably stabilized by ribosome–nascent chain interactions when the TMS reached that location.

### Loop size does not affect folding
To determine whether the size of the TMS1–TMS2 separation had any effect on the timing of TMS2 folding, integration intermediates were prepared with nascent chains that had a longer loop between the TMSs (Fig. 2 A). The low E measured with 2TM$_{L53}$DA2$_{163}$ integration intermediates showed that extending the polypeptide by 41 residues (∼140 Å if fully extended) did not cause the newly synthesized TMS2 to fold (Fig. 2 F). However, when the C terminus of TMS2 was 6 residues from the PTC, E increased sharply to 30% (Fig. 2 F). Thus, nascent chain folding inside the ribosome tunnel was independent of the length of the nascent chain, as folding occurred only after a TMS entered the ribosome tunnel and reached a certain location.

### Folded TMS2 is helical
Because the two dyes are covalently attached to the peptide backbone by long flexible tethers, the FRET approach cannot determine directly the conformation of the intervening polypeptide. However, one can compare the dye separations when TMS2 is in the ribosome tunnel and when TMS2 is folded into a transmembrane α-helix in the nonpolar core of the bilayer. After 2TM$_{L12}$DA2 was fully translated and released from the translocon into the lipid bilayer, E was 31% for TMS2 with donor and acceptor dyes on opposite sides of the membrane (Fig. 2 E). This E was experimentally indistinguishable from the E values measured for TMS2 inside the tunnel when the nascent chain was 126 residues or longer, suggesting that TMS2 folds into an α-helix or an equivalently compact structure inside the ribosome tunnel.

### TMS3 folds in the ribosome tunnel
TMS3, the third TMS segment in a PMP, has an orientation in the bilayer opposite to that of TMS2. Lin et al. (2011) showed that the entry of TMS3 into the tunnel triggered the reversal of the RTC structural changes elicited by TMS2. Because TMS1 and TMS2 each folded shortly after entering the tunnel, we determined whether TMS3 also folded. The E for RTCs containing 3TM$_{L12,18}$DA3$_{159}$ nascent chains (Fig. 3 A) was 5% (Fig. 3 B), so TMS3 was fully extended when newly synthesized. However, E was 37% for 3TM$_{L12,18}$DA3$_{167}$ RTCs (Fig. 3 B; dye separation

Table II. **Dye anisotropies in the ribosomal tunnel and at the membrane[a]**

| PMP RTC | Dye location | NBD r[b] | BOP r[c] |
|---|---|---|---|
| $2TM_{L12}DA2_{122}$ | Tunnel | 0.31 ± 0.01 | 0.30 ± 0.01 |
| $2TM_{L12}DA2_{125}$ | Tunnel | 0.30 ± 0.01 | 0.30 ± 0.02 |
| $2TM_{L12}DA2_{126}$ | Tunnel | 0.28 ± 0.02 | 0.29 ± 0.02 |
| $2TM_{L12}DA2_{130}$ | Tunnel | 0.29 ± 0.01 | 0.29 ± 0.01 |
| $2TM_{L12}DA2_{FL}$[d] | Membrane[e] | 0.27 ± 0.03 | 0.29 ± 0.01 |
| $3TM_{L12,18}DA3_{159}$ | Tunnel | 0.30 ± 0.03 | 0.28 ± 0.01 |
| $3TM_{L12,18}DA3_{163}$ | Tunnel | 0.29 ± 0.02 | 0.29 ± 0.01 |
| $3TM_{L12,18}DA3_{167}$ | Tunnel | 0.29 ± 0.03 | 0.29 ± 0.01 |

[a]Data are the average ± SD for three or more independent experiments.
[b]NBD: $\lambda_{ex}$ = 468 nm, $\lambda_{em}$ = 530 nm, bandpass = 4 nm; measured in absence of acceptor.
[c]BOP, $\lambda_{ex}$ = 575 nm, $\lambda_{em}$ = 595 nm, bandpass = 4 nm; measured in absence of donor.
[d]Full-length $2TM_{L12}DA2$ proteins were translated, released from the translocon, and integrated into the ER membrane.
[e]Dyes are at opposite surfaces of ER membrane, with donor in lumen and acceptor in cytosol.

was 21 residues in TMS3 and 24 in TMS2), indicating that TMS3 had folded into a compact conformation when its C terminus was 6 residues from the PTC. Thus, TMS1, TMS2, and TMS3 each folded into a compact, largely helical conformation when its C terminus was 6–7 residues from the PTC, even though the TMSs differed markedly in length, sequence, hydrophobicity, charged residues, and final bilayer orientation (Fig. S1).

### TMS folding is ribosome induced

The folding of successive TMSs at the same location in the tunnel suggested that the ribosome plays an active role in nucleating and stabilizing TMS folding. To examine this issue directly, FRET-detected folding of TMS2 inside and outside of the ribosome tunnel was compared. Parallel RNC samples with either $2TM_{L12}DA2_{130}$ or $2TM_{L12}DA2_{180}$ nascent chains were prepared in the absence of ER microsomes and SRP to yield RNCs with TMS2 located either inside the tunnel or in the solvent outside the tunnel (Fig. 4 A). Spectral analysis of $2TM_{L12}DA2_{130}$ RNCs revealed that TMS2 was folded (E = 21%; Fig. 4 B) in the tunnel

(this E with free RNCs was somewhat lower than the 29% observed with membrane-bound RNCs). In contrast, the TMS2 sequence of $2TM_{L12}DA2_{180}$ was completely unfolded and extended after emerging from the tunnel (E = 4%; Fig. 4 B), despite the presence of cytosolic chaperones. Thus, the TMS2 sequence folded stably inside the aqueous (Crowley et al., 1993) ribosome tunnel, but not outside the ribosome in the aqueous medium. The ribosome therefore actively induces and stabilizes the folding of TMS2.

### TMS2 photocrosslinks ribosomal protein L4

To determine whether TMS2 was adjacent to ribosomal proteins inside the tunnel, integration intermediates were prepared in the dark with a photoreactive probe in TMS2 and then illuminated to initiate cross-linking to nearby molecules. By varying the distance between the PTC and the TMS2 probe, TMS proximity to ribosomal proteins could be determined at different stages of integration. Probes were incorporated into a specific site of TMS2 by adding $N^{\varepsilon}$-(5-azido-2-nitrobenzoyl)-Lys-tRNA$^{Lys}$ ($\varepsilon$ANB-Lys-tRNA$^{Lys}$) to an in vitro translation of $2TM_{L12}K2$



**A**
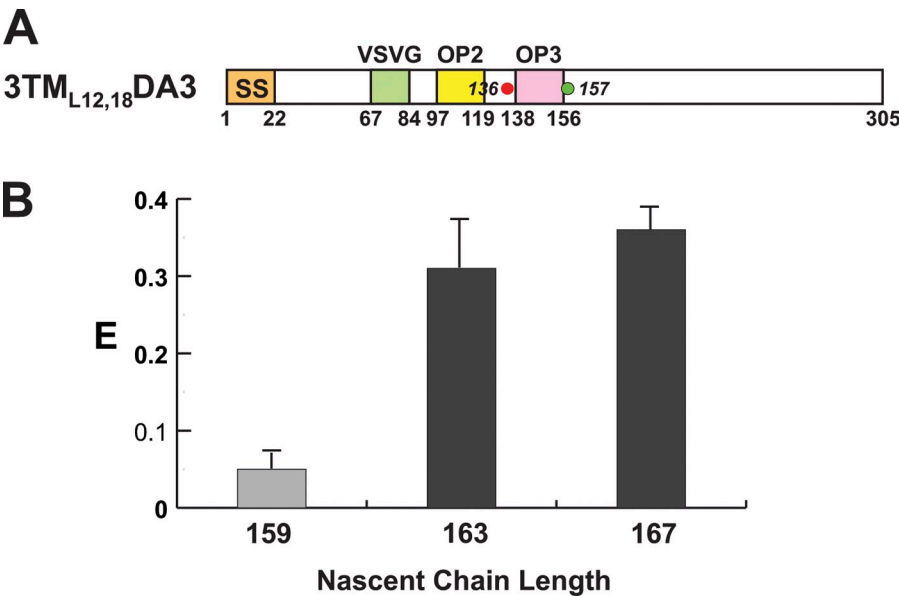$3TM_{L12,18}DA3$

**B**

Figure 3. **FRET-detected TMS3 folding.** (A) Topogenic sequence and dye locations are depicted as in Fig. 2. TMS3 = opsin 3 (magenta). (B) Average E (±SD) values obtained in three or more independent experiments for $3TM_{L12,18}DA3$ RTCs with different nascent chain lengths and folded (black) or unfolded (gray) TMSs.

(K2 indicates the single Lys codon is located in TMS2). Because εANB-Lys is uncharged, TMS hydrophobicity was retained. To examine TMS2 environment at higher resolution, probes were placed at four adjacent TMS2 sites (1 site/sample; Fig. S1). This approach allowed us to determine whether any observed proximity was random or specific because the probes would project from different sides of a folded TMS helix (McCormick et al., 2003).

When four different probe sites (106–109; Fig. S1) were examined in parallel at each of four different lengths (122, 125, 126, 130) of $^{35}$S-labeled nascent $2TM_{L12}K2$, relatively few high molecular mass radioactive bands were observed in SDS gels of total sample proteins from either membrane-bound RTCs (Fig. 5 A) or free RNCs (Fig. 5 B). Because the high molecular mass bands were absent in samples that lacked the ANB probe or were not illuminated, these bands resulted from nascent chain photocrosslinking to proteins inside the ribosome tunnel. The primary photocrosslinking target for all probe sites and nascent chain lengths for both RTCs and RNCs was a 40-kD protein, most likely ribosomal protein L4. No antibodies are available to confirm this identification by immunoprecipitation, but L4 has a molecular mass near 40 kD and is the largest protein exposed inside the 60S tunnel (Armache et al., 2010b; Ben-Shem et al., 2010).

Interestingly, the extent of TMS2 cross-linking to L4 was the same from all four probe sites, irrespective of the length of the nascent chain. Because L4 does not circumscribe the ribosome tunnel and instead is exposed only on one side, the fact that L4 was photocrosslinked equally well from each of the four different probe locations in TMS2 (Fig. 5, A and B) reveals that nascent chains in the tunnel were oriented randomly relative to L4. Moreover, the insensitivity of photoadduct formation to nascent chain length indicates that similar numbers of TMS2 probes were adjacent to L4 during photolysis of nascent chains 122–130 residues long. Because the number of TMS2 probes reacting with L4 did not change as the nascent chain was lengthened by 8 residues, it appears that the extent of dynamic back and forth motion of individual nascent chains in the ribosome tunnel was sufficient to equalize the average probe concentration next to L4. Thus, the nascent chains that react covalently with L4 are moving and rotating freely in the ribosome tunnel, and are not bound to its surface. TMS2 photocrosslinking to L4 in the tunnel therefore results from a random and dynamically constant spatial proximity over this range of nascent chain lengths, not from TMS2-L4 association.

### TMS2 is adjacent to L17 and L39

TMS2 also photocrosslinked to smaller proteins with masses near 18 or 7 kD (Fig. 5, A and B), most likely L17 (18 kD) and L39 (7 kD) because these are the only proteins besides L4 exposed inside the eukaryotic ribosome tunnel (Armache et al., 2010b; Ben-Shem et al., 2010). Yet the electrophoretic mobilities of the two smaller photoadduct bands in lanes 9 and 13 are distinctly different from those in lanes 10 and 14 (Fig. 5, A and B), raising the possibility that probes in different TMS2 positions cross-linked to different proteins. To ascertain whether either or both of the photoadduct bands near 30 kD in lanes 9
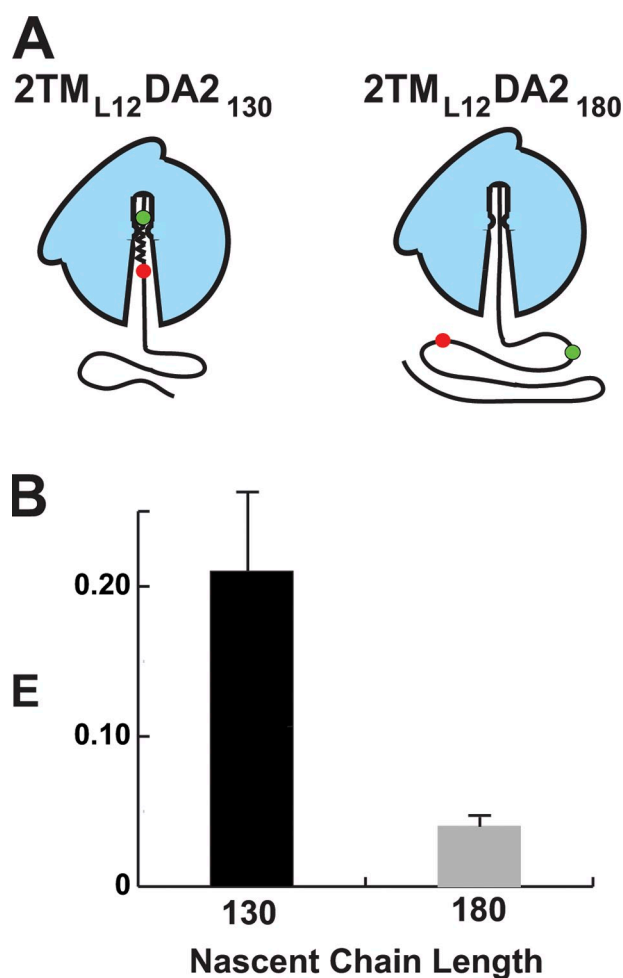
Figure 4. **TMS folding is ribosome dependent.** (A) The approximate locations of donor (green) and acceptor (red) dyes in $2TM_{L12}DA2_{130}$ and $2TM_{L12}DA2_{180}$ RTCs are shown. (B) Average E (±SD) values obtained in three or more independent experiments for these RTCs with folded (black) or unfolded (gray) TMSs.

and 10 of Fig. 5 A contained L17, samples were photolyzed and immunoprecipitated with antibodies specific for L17. The results shown in Fig. 5 C reveal that the 106 and 107 photoadducts each contained both L17 and the radioactive nascent chain. Thus, TMS2 cross-links to L17 from both the 106 and 107 probe sites.

No antibodies are available to immunoprecipitate L39, but the probes at 106 and 107 also appear to react covalently with L39 (Fig. 5 A).

### TMS2 folding coincides with its exposure to L17

The extent of TMS2-L17 photocrosslinking varied with nascent chain length because the ∼30-kD photoadduct yield was close to zero with 122mers, maximal with 126mers and 130mers, and 22% of maximal for 125mers; the yields of putative TMS2-L39 photoadduct varied similarly (Fig. 5, A and B). The sharp increase in L17 and L39 photocrosslinking as the nascent chain lengthened by a single residue is striking, especially given the insensitivity of L4 photocrosslinking to nascent chain length between 122 and 130. Equally striking was the folding of TMS2

Figure 5. **TMS2 photocrosslinking to ribosomal proteins.** Membrane-bound (A) or free (B) RNCs containing nascent $^{35}$S-labeled $2TM_{L12}K2$ chains of different lengths were prepared with a photoreactive probe at one of four different TMS2 sites (106–109; Fig. S1), photolyzed, and analyzed by SDS-PAGE. Photoadducts containing L4, L17, and L39 are identified by ■, ●, and ▲, respectively. (C) Free RNCs containing a $^{35}$S-labeled $2TM_{L12}K2_{126}$ nascent chain with a probe at either 106 or 107 were photolyzed and analyzed (lanes 1 and 2 = total proteins; lanes 3 and 4 = proteins precipitated with antibodies specific for L17).
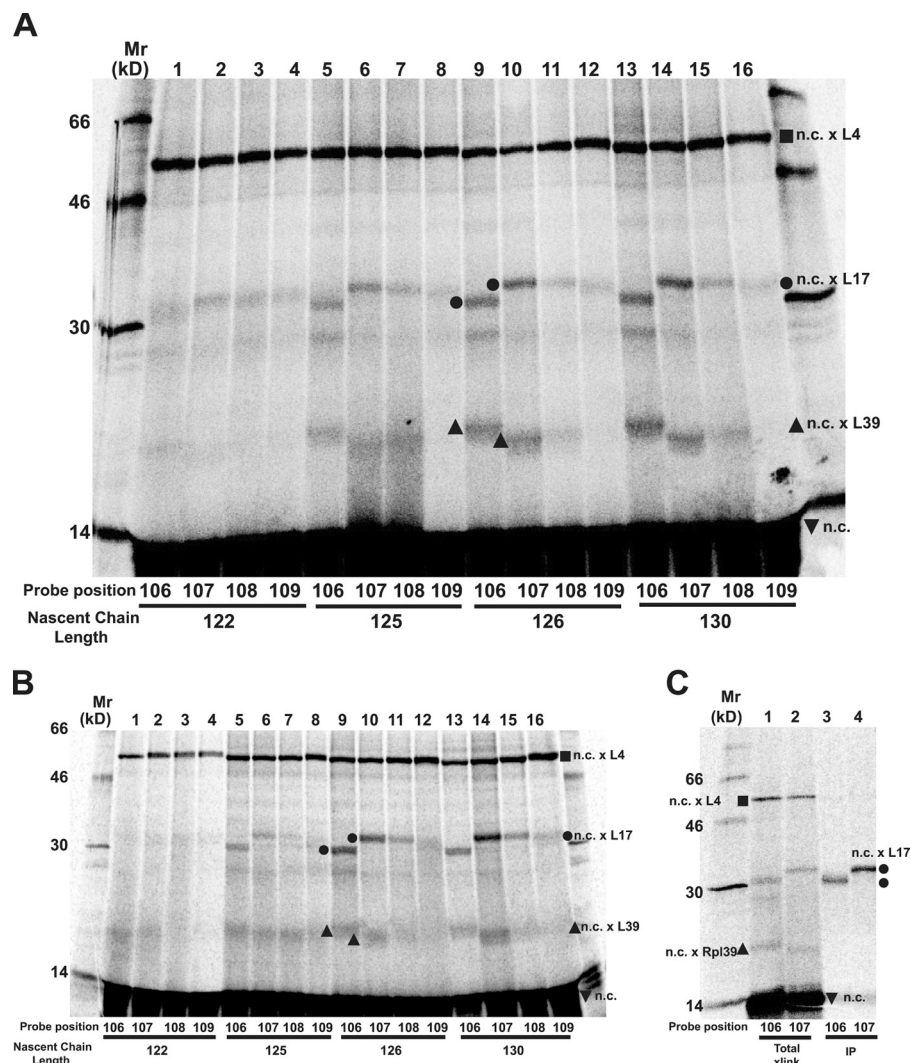


into a helical conformation when $2TM_{L12}K2$ reached a length of 126 residues (Fig. 2 E). The very strong correlation between the changes in TMS2 conformation and environment strongly suggests that TMS folding and TMS accessibility to L17 are linked, and that only folded TMSs are adjacent to L17. Furthermore, because the nascent chain length dependence of TMS2-L17 photocrosslinking was the same for both membrane-bound RTCs (Fig. 5 A) and free RNCs (Fig. 5 B), ribosome-induced TMS folding and access to L17 is an intrinsic property of all ribosomes, not just membrane-bound ribosomes.

### Helical TMS2 binds to L17 in a specific orientation

L4 was randomly and uniformly cross-linked from four different probe sites in TMS2 (Fig. 5 A), but TMS2 photocrosslinking to L17 was very specific and nonrandom when TMS2 was folded into a helical conformation in 126- and 130-residue nascent chains. Probes at 106 and 107 both cross-linked efficiently to L17, whereas very little cross-linking was observed with probes at 108 and 109 (Fig. 5, A and C). This result suggests that the helical surfaces from which the 106 and 107 probes projected were facing L17, whereas the probes at 108 and 109

projected into the aqueous ribosome tunnel or reacted with rRNA (cross-linking to rRNA was not examined in this study).

The different electrophoretic mobilities of the 106 and 107 photoadducts (Fig. 5 C) are best explained by the probes at 106 and 107 reacting with two different sites on L17 (Plath et al., 1998). Furthermore, because lanes 9 and 13 contained only a single radioactive 30-kD band (Fig. 5 A), the 106 probe was always located in the same position relative to L17, and never reacted with L17 near where the 107 probe was always located. It therefore appears that the adjacent TMS2 106 and 107 probes/residues in the TMS2 helix each projected toward distinct, nonoverlapping regions of L17. The only mechanism by which TMS2 and its probes could stably and reproducibly occupy the same position in the ribosome tunnel adjacent to L17 is if TMS2 were bound to specific ribosomal components and held in a fixed orientation (McCormick et al., 2003). The specificity of L17 cross-linking to TMS2 therefore strongly indicates that helical TMS2 binds to the tunnel surface adjacent to L17.

### Dynamic TMS location and conformation

L4, L17, and L39 are exposed to the aqueous nascent chain pathway at different locations inside the ribosome tunnel
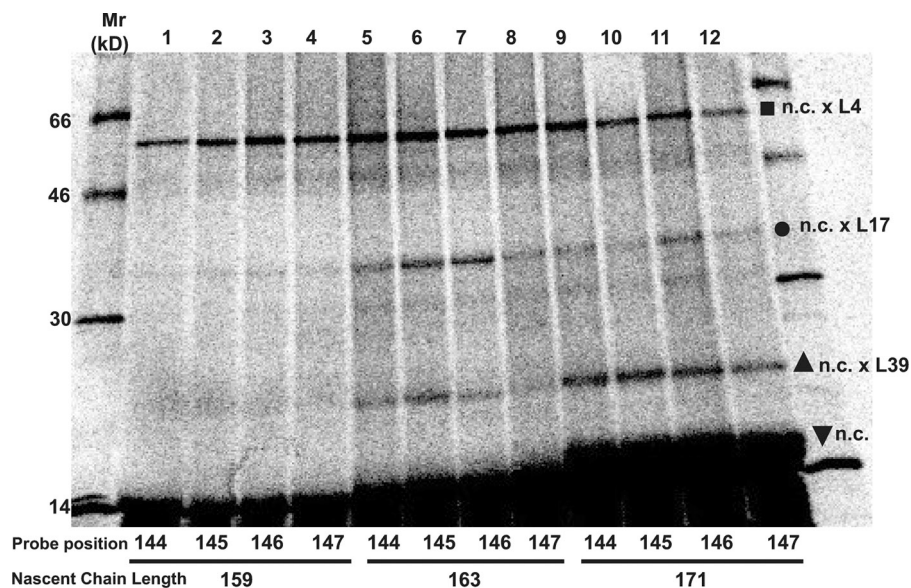
Figure 6. **TMS3 proximity to ribosomal proteins.** Free RNCs containing nascent $^{35}$S-labeled $3TM_{L12,18}K3$ chains of different lengths were prepared with a photoreactive probe at one of four different TMS3 sites (144–147; Fig. S1) and photolyzed. Photoadducts are identified as in Fig. 5.

Gel labels:
- ■ n.c. x L4
- ● n.c. x L17
- ▲ n.c. x L39
- ▼ n.c.

Probe position: 144 145 146 147 | 144 145 146 147 | 144 145 146 147
Nascent Chain Length: 159 | 163 | 171

(Armache et al., 2010b; Ben-Shem et al., 2010), yet $2TM_{L12}K2_{126}$ and $2TM_{L12}K2_{130}$ nascent chains with probes at either 106 or 107 in TMS2 form photoadducts with L4, L17, and L39 in the same sample (Fig. 5, A and B). Because each nascent chain has only a single probe, each sample contains TMS2 sequences that are adjacent to each target protein at the time of photolysis. For TMS2s to be positioned at different ribosome tunnel locations at the same time, the nascent chains must be dynamically diffusing back and forth in the ribosome tunnel. However, the distribution of TMS2s inside the tunnel cannot be determined from the relative band intensities because photoadduct yield is critically dependent on the unknown efficiency of probe reaction with exposed ribosomal protein residue(s) and the extent of their exposure to the tunnel.

TMS2 conformation also varies dynamically inside the ribosome tunnel. TMS2 photocrosslinked to L4 while unfolded and oriented randomly, whereas L17 was photocrosslinked when folded TMS2 is bound to the tunnel wall in a specific orientation. Thus, each RTC sample contained folded and unfolded TMS2 sequences. The apparently facile transition between helical and unfolded TMS2 conformational states does not conflict with the FRET data because the E values are averages. The measured E values therefore reflect the predominant, but not the only, conformation at a given nascent chain length (Fig. 2 E).

### Folded TMS3 photocrosslinks L17

When photoreactive probes were positioned at each of four TMS3 sites in $3TM_{L12,18}K3$ nascent chains of different lengths (one site/sample; Fig. S1), the photocrosslinking pattern was very similar to that observed with TMS2 probes: L4 was crosslinked equally from each of the four TMS3 sites, indicating that those nascent chains were rotating randomly and freely in the tunnel when illuminated; photoadducts containing L17 and L39 were detected only after the TMS3 folded (i.e., in nascent chains 163 residues or longer); and L17 photocrosslinking was asymmetric because probes at 145 and 146 cross-linked

more efficiently to L17 than probes at 144 and 147 (Fig. 6). Thus, folded TMS3 appears to be adjacent to and photocrosslink L17 and L39 after binding to the ribosome tunnel surface in a specific orientation.

Interestingly, the two TMS3-L17 photoadducts did not differ significantly in electrophoretic mobility. Hence, it appears that TMS2 and TMS3 do not bind adjacent to L17 in the same way, a result that is not surprising given their different sequences and hence binding surfaces.

### TMS folding correlates with RTC changes

Three experimentally detectable events occurred when the $2TM_{L12}$ nascent chain reached a length of 126 residues: TMS2 folded into a helix (Fig. 2 E), TMS2 bound to the ribosome tunnel surface adjacent to L17 (Fig. 5 A), and TMS2 exposure switched from cytosolic to lumenal (Lin et al., 2011), as depicted in Fig. 7. The coincidence of these events was not accidental because changing the loop size did not uncouple these three events (Fig. 2 F; Lin et al., 2011). TMS3 triggered similar events when a $3TM_{L12,18}$ nascent chain reached a length of 163 residues: TMS3 folded into a helix (Fig. 3 B), TMS3 bound to L17 (Fig. 6), and TMS3 exposure changed from lumenal to cytosolic (Lin et al., 2011). TMS1 movement into the ribosomal tunnel and folding elicited the same changes as did TMS3 (Liao et al., 1997; Woolhead et al., 2004). Although these three events, TMS folding, TMS binding to L17, and an inversion of TMS exposure to cytosol or lumen, were temporally coincident for each of three successive TMSs, they were not spatially coincident: TMS folding and binding to L17 occurred at the constriction far inside the ribosome tunnel, while the lumenal end of the aqueous translocon pore was alternately closed or opened on the opposite side of the ER membrane.

To coordinate the timing of events separated by more than 110Å, a molecular linkage that extends from the tunnel constriction through the ribosome and membrane to the ER lumen must exist and act as a signal transduction pathway. Furthermore, because these structural changes occur only after the C-terminal
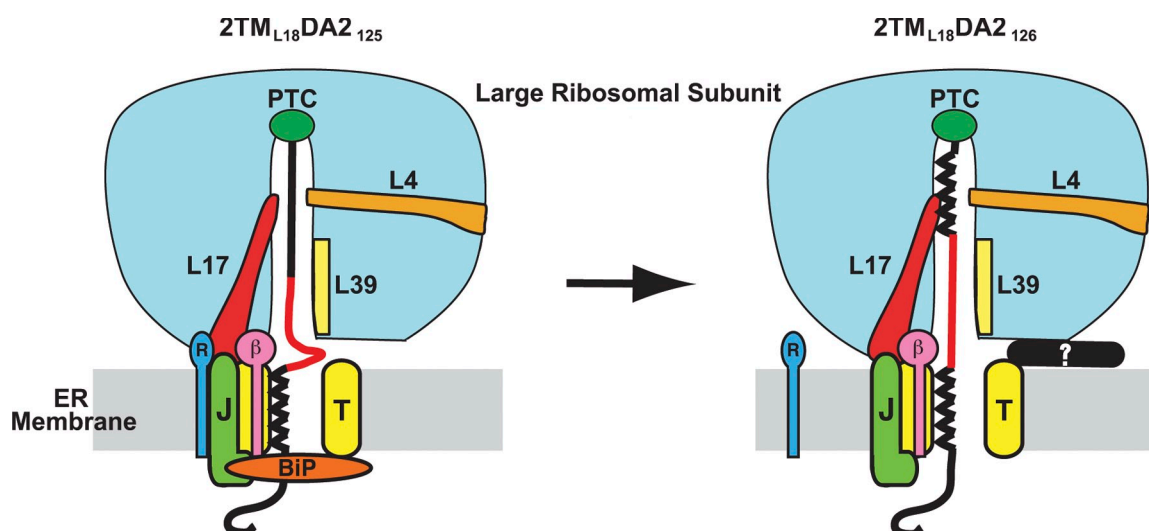
Figure 7. **L17 links TMS folding with changes in the RTC.** TMS2 folding coincides with its binding to L17 (red) and also with a change in nascent chain exposure from cytosolic to lumenal, strongly suggesting that L17, which extends from the constriction to the ribosome surface near the translocon (T, yellow), acts as a conduit for communicating the imminent arrival of a TMS at the translocon. Although this cartoon depicts the ribosome tunnel as fully sealed off from the cytosol when TMS2 is still far inside the tunnel, this is unlikely to be the case in vivo because ongoing translation will move TMS2 down the tunnel as the RTC and other molecules are assembled and rearranged at the membrane. Thus, TMS2 is likely to be in or near the translocon by the time the depicted changes are completed. Cytosolic access to the ribosome tunnel is blocked either by a conformational change in the RTC and/or by an unknown protein (?, black), here shown binding to the RTC to block tunnel access. BiP-mediated pore closure is reversed by ATP-dependent release of BiP from an unidentified J domain–containing ER membrane protein (J, green; Alder et al., 2005). RAMP4 (R, dark blue) is adjacent to L17 when the nascent chain is exposed to the cytosol, whereas Sec61β (β, magenta) is adjacent to the nascent chain throughout (Pool, 2009).

end of a nascent chain TMS has moved 6–7 residues into the ribosome tunnel and folded, the data indicate that nascent chain folding initiates and thereby regulates what happens at each end of the translocon pore.

### A non-TMS helical sequence does not fold early in the tunnel

Prolactin folds into a four-helix bundle (Teilum et al., 2005), and these four non-TMS helices did not trigger RTC changes as they passed through the RTC (Crowley et al., 1994). The full-length protein folded after release into the lumen, as shown by FRET (E = 25%; Fig. 1 E) between dyes that flanked helix 2 (Fig. 1 C, triangles). However, E was 3% when the C terminus of helix 2 was 8 residues from the PTC. Because no helix 2 folding was detected where TMS helices folded, the ribosome appears to distinguish between TMSs and non-TMS helices at the tunnel site that initiates RTC changes. E then increased to 13% after approximately half of helix 2 had exited the tunnel, presumably because helix 2 began to fold near the tunnel exit (Kosolapov and Deutsch, 2009).

## Discussion

The data reported here and in the accompanying paper (Lin et al., 2011) provide several structural, functional, and mechanistic insights into the cotranslational integration of PMPs into the ER membrane. The primary observations include: each successive PMP nascent chain TMS folds into a compact conformation inside the ribosome tunnel (Fig. 2, E and F; and Fig. 3 B); each TMS folds abruptly when its C terminus is 6–7 residues from the PTC, irrespective of loop size (Fig. 2, E and F; and

Fig. 3 B); TMS folding is induced and stabilized by the ribosome (Fig. 4 B); nonpolar sequences of various lengths, sequences, hydrophobicities, and bilayer orientations are recognized by the ribosome as TMSs and fold (Figs. S1, 2 E, and 3 B; Lin et al., 2011); nascent PMP TMS location and conformation vary dynamically within the ribosome tunnel (Figs. 5 and 6); free and randomly oriented nascent chain TMSs in the aqueous ribosome tunnel photocrosslink to L4, whereas TMSs bound to the tunnel surface photocrosslink both L17 and L39 (Figs. 5 and 6); bound TMS2s always orient with the same two probes facing different portions of L17 (Fig. 5); and TMSs fold (Figs. 2 E and 3 B) and bind to the ribosome tunnel (Figs. 5 and 6) at the same nascent chain length at which RTC structural changes occur in and on both sides of the ER membrane (Lin et al., 2011).

When combined, these separate observations suggest the following scenario. Similar to a polypeptide lacking TMSs that moves through the ribosome tunnel in an extended conformation and does not bind to L17 (Fig. 1 D; Woolhead et al., 2004), a newly synthesized TMS sequence of a nascent membrane protein is extended as it enters the tunnel (Fig. 2 E). However, a TMS binds to the tunnel upon reaching a specific location adjacent to L17 and is induced to fold into a compact conformation that appears α-helical. Such binding is transient, as it must be as translation proceeds in vivo. Thus, nascent chain TMS conformation and location are best described as dynamic inside the ribosome tunnel, moving back and forth while shifting between two states: bound and folded versus free and unfolded. A specific interaction between the ribosome tunnel and the TMS presumably stabilizes the binding and shifts the dynamic equilibrium to the FRET-detected folded state.

Similar to the heterogeneity in ribosomal protein photo-crosslinking targets observed with both eukaryotic (Figs. 5 and 6; Woolhead et al., 2004) and bacterial (Houben et al., 2005) nascent chains, Brimacombe and colleagues found that a photoreactive probe at the N-terminal end of an ∼30-residue nascent chain photocrosslinked to rRNA nucleotides all along the ribosome tunnel, including near the PTC (Stade et al., 1995; Choi and Brimacombe, 1998; Choi et al., 1998). Because radioactive amino acids at each end of the nascent chain ensured that only polypeptides of the desired length were examined in these studies, even relatively long nascent chains were shown to fold back inside the ribosome tunnel toward the PTC. The combined photocrosslinking data therefore reveal that, despite the obvious spatial constraints, nascent chain positioning varies dynamically and significantly within the ribosome tunnel.

The functional ramifications of TMS folding are revealed by the striking coincidence of three spatially separated events: TMS folding, TMS binding to L17, and major structural rearrangements at the ER membrane. TMS folding and binding inside the ribosome tunnel appears to be communicated to the membrane by a long transmembrane signal transduction pathway that most likely involves L17 and rRNA, macromolecules that extend from the tunnel constriction to the membrane surface (Armache et al., 2010a,b; Ben-Shem et al., 2010). The binding of folded TMSs at the constriction presumably triggers L17 and/or rRNA conformational changes that directly or indirectly alter the structures and interactions of RTC components in and on both sides of the ER membrane (Fig. 7).

Each successive TMS folding event inverts RTC structure, thereby alternating nascent chain exposure and PMP loop delivery between lumen and cytosol (Lin et al., 2011). TMSs therefore initiate RTC structural changes, but do not control their nature (lumenal or cytosolic loop deployment). Instead, the RTC must retain a molecular "memory" that ensures the repetitive alternation of two structural states and the cyclical coordination of ribosomes and multiple proteins in and on both sides of the membrane during cotranslational PMP integration. The mechanistic basis of such a molecular memory is most likely an obligatory alternation between two RTC structures at the membrane, similar to the elongation factor–dependent cycling of the RNC conformation between two different states, EF-Tu binding and EF-G binding, during translation.

Each pore opening/closing involves multiple molecules in and on both sides of the ER membrane, including the coupled RTC, BiP (Haigh and Johnson, 2002), calmodulin (Erdmann et al., 2011), RAMP4 (Pool, 2009), and an unknown J domain protein that binds BiP (Alder et al., 2005). These proteins must act in the proper sequence to achieve RTC inversion without compromising membrane integrity, and such obligatory sequencing requires time. The time available for the inversion of nascent chain exposure is dictated by the 4–6 aa/sec rate of translation during cotranslational integration (Braakman et al., 1991; Ujvári et al., 2001; Cheng and Gilmore, 2006).

To trap a sample at a discrete stage of integration, we used truncated mRNAs. Although this approach is insensitive to the kinetics of individual steps, it did allow us to determine when (at what nascent chain length) each step can be accomplished or accommodated by the RTC. For example, each TMS folded when its C terminus was 6–7 residues from the PTC, and this event triggered the complete inversion of RTC structure and translocon pore exposure (Lin et al., 2011). Thus, once initiated, these structural rearrangements proceeded to completion and were not dependent on translation. Given this result and the dynamics of nascent chain conformation and location in the ribosome tunnel, it seems likely that RTC inversion is initiated without TMS binding to the L17 site for an extended period. Instead, after triggering RTC changes, the TMS moves another 25–30 residues through the tunnel before entering the translocon. Thus, any structural changes at the RTC and membrane initiated by a TMS at L17 have to be completed within 5–6 s to avoid directing the nascent polypeptide following the TMS into the wrong compartment.

Given this short time, the necessity of recognizing nascent chain TMSs far inside the ribosome tunnel is clearly evident: early initiation of the collection and coordination of components involved in RTC cycling ensures that RTC changes are complete before TMS entry into the translocon. The permeability barrier is therefore maintained and PMP loops are directed to the proper side of the membrane as translation proceeds in vivo. Even with this "early warning" system, variations in protease-detected exposure of nascent membrane proteins to the cytosol observed in vivo suggest that translation proceeds faster than conformational changes at the translocon during gating (Cheng and Gilmore, 2006).

The ribosome tunnel surface is not uniform (Lu et al., 2007; Armache et al., 2010b; Ben-Shem et al., 2010), and nascent chain folding has been detected in the tunnel at various locations (Lu and Deutsch, 2005a; Bhushan et al., 2010a; Wilson and Beckmann, 2011). TMS folding is ribosome induced (Fig. 4 B) and is initiated at the same location (when TMS C terminus is 6–7 residues from the PTC; Fig. 2, E and F; and Fig. 3 B), probably by a combination of entropic effects resulting from the confinement of the nascent chain within the tunnel (Ziv et al., 2005) and of direct contacts between TMSs and ribosomal components at a specific site(s) within the tunnel. The ribosomal components other than L17 that interact with the TMS inside the tunnel have yet to be identified (Figs. 5 and 6), but fluorescence lifetime data with the environmentally sensitive NBD dye (Johnson, 2005b) indicate that the site has a nonpolar character (Table I; Lin et al., 2011). No nonpolar surfaces were observed in the archaeal 50S crystal structure tunnel (Nissen et al., 2000), but the extended β-hairpin tip of L22 (the prokaryotic homologue of L17) underwent a ligand binding–dependent conformational change in the tunnel (Berisio et al., 2003). Nascent chain interactions with ribosomes also alter the conformation of tunnel-exposed rRNA nucleotides (Bhushan et al., 2010b; Vázquez-Laslop et al., 2010). Because translating and nontranslating ribosomes have different conformations (Flanagan et al., 2003; Bornemann et al., 2008), the lifetime-detected nonpolar environment for TMSs inside the ribosome tunnel most likely arises from transient or static conformational changes in translating ribosomes that expose L17 residues and/or rRNA bases.

Although each of the three TMSs examined here folded into compact structures near L17, and TMS3 folding in native aquaporin was detected by nascent chain photocrosslinking to translocon proteins (Daniel et al., 2008), chemical reactivity data did not detect any folding of the TMSs of a native PMP, Kv1.3, until near the ribosomal tunnel exit in free RNCs (Tu and Deutsch, 2010). The simplest explanation for these differences is that not all TMSs fold when passing through the ribosome tunnel and/or folding differs in free and membrane-bound ribosomes. Further experimentation will be required to assess the generality of TMS and non-TMS nascent chain folding at L17, as well as whether non-TMSs can ever initiate RTC structural changes.

Nascent chain folding into compact conformations within the ribosome tunnel has now been reported using a variety of techniques, including FRET (Woolhead et al., 2004, 2006; this paper), cryoEM (Gilbert et al., 2004; Seidelt et al., 2009; Bhushan et al., 2010a,b, 2011), chemical reactivity (Lu and Deutsch, 2005a,b; Kosolapov and Deutsch, 2009; Tu and Deutsch, 2010), glycosylation (Mingarro et al., 2000; Tu and Deutsch, 2010), photocrosslinking (Daniel et al., 2008), and chemical cross-linking (Peterson et al., 2010). Nascent chain TMSs (Woolhead et al., 2004; this paper) and sequences in SecM (Nakatogawa and Ito, 2002; Bhushan et al., 2011), TnaC (Seidelt et al., 2009), and arginine attenuator peptide (Bhushan et al., 2010b) appear to interact with the tunnel constriction formed by L4 and L17 (L22), though the contacts may differ for different nascent chains (Bhushan et al., 2010b). In each case, the bound nascent chains act as regulatory elements, though in different directions: the TMSs in membrane-bounds RTCs act ahead to regulate PMP loop trafficking into the cytosol or lumen, whereas SecM (Nakatogawa and Ito, 2002), TnaC (Gong and Yanofsky, 2002), arginine acceptor protein (Fang et al., 2004), and other nascent chains (Ito et al., 2010; Cruz-Vera et al., 2011) in free RNCs act backward to arrest translation. Nascent chain interactions with the ribosome therefore play a critical role in regulating both translation and trafficking, and ribosome-induced or -stabilized nascent chain binding and/or folding appears to be the mechanism by which the ribosome distinguishes between relevant and irrelevant sequences in the normally extended nascent chain.

## Materials and methods

### Plasmids, mRNA, and tRNAs
Using standard techniques, PMP plasmids were constructed from lysine-free bovine preprolactin (pPL; each Lys in PL was converted to Q by site-directed mutagenesis) and lysine-free coding sequences within the genes for vesicular stomatitis virus G protein (VSVG), bovine opsin (OP, a gift from Dr. R. Gilmore, University of Massachusetts Medical School, Worcester, MA), yeast invertase 2, and human Bcl-2, as detailed below. A single amber and a single Lys codon were introduced into the coding sequence of each PMP using QuikChange (Agilent Technologies) to incorporate the acceptor and donor dye, respectively, at specific sites in 2TM and 3TM as described for pPLDA and 111pDA (Woolhead et al., 2004). To avoid ambiguity in interpreting RTC structural changes during integration, fusion proteins were designed with a cleavable signal sequence sufficiently far from the first TMS that RNC targeting to the translocon would be completed before the entire TMS was synthesized. The N terminus of each membrane protein in this study was therefore comprised of the first 63 residues of pPL modified to remove the lysines in its signal sequence (Crowley et al., 1994;

Woolhead et al., 2004). When translated, full-length 111p SSMP contained, from N to C terminus, the pPL fragment, VSVG TMS, invertase 2 (residues 96–130), Bcl-2 (residues 82–141 and 153–182), and lysine-free linkers (Johnson et al., 1995; Do et al., 1996). Full-length $2TM_{L12}$ contained the pPL fragment, VSVG TMS, a 12-residue hydrophilic linker, OP2 TMS, opsin (residues 97–116, the loop following OP2), invertase 2 (residues 96–130), Bcl-2 (residues 92–182), and lysine-free linkers. $2TM_{L53}$ differed from $2TM_{L12}$ only in the loop, where a pPL segment (residues 49–96 with the two Ks mutated to Qs) and linker residues replaced the 12-residue loop. Full-length $3TM_{L12,18}$ contained the pPL fragment, VSVG TMS, a 12-residue hydrophilic linker, opsin (residues 74–133 contain the OP2 TMS, the natural intervening loop, and the OP3 TMS), invertase 2 (residues 96–130), Bcl-2 (residues 92–182), and lysine-free linkers. The invertase 2 sequence contained three N-linked glycosylation sites that served as a marker for whether that polypeptide segment was lumenal (glycosylated) or cytosolic (not glycosylated). Primary sequences were confirmed by DNA sequencing. Truncated mRNAs were transcribed in vitro using SP6 polymerase and PCR-produced DNA fragments of the desired length.

Yeast [$^{14}$C]Lys-tRNA$^{Lys}$ was reacted (0°C, 14–25 s at high pH [varies with probe]) with the N-hydroxysuccinimide ester of acetic acid, 6-(7-nitrobenz-2-oxa-1,3-diazol-4-yl)aminohexanoic acid (Invitrogen), 5-azido-2-nitrobenzoic acid (Thermo Fisher Scientific), or 4,4-difluoro-5, 7-dimethyl-4-bora-3a,4a-diaza-s-indacene-3-propionic acid (Invitrogen) to yield N$^{ε}$-acetyl-Lys-tRNA$^{Lys}$ ($ε$Ac-Lys-tRNA$^{Lys}$), N$^{ε}$-6(7-nitrobenz-2-oxa-1,3-diazol-4-yl)aminohexanoyl-Lys-tRNA$^{Lys}$ ($ε$NBD-Lys-tRNA$^{Lys}$), N$^{ε}$-(5-azido-2-nitrobenzoyl)-Lys-tRNA$^{Lys}$ ($ε$ANB-Lys-tRNA$^{Lys}$), or N$^{ε}$-(BODIPY FL)-Lys-tRNA$^{Lys}$ ($ε$BOF-Lys-tRNA$^{Lys}$), respectively (Johnson et al., 1976; Krieg et al., 1986; Crowley et al., 1993; Woolhead et al., 2004). Similarly, [$^{3}$H]Lys-tRNA$^{amb}$ was reacted with the N-hydroxysuccimide ester of acetic acid or 4,4-difluoro-5-(2-pyrrolyl)-4-bora-3a,4a-diaza-s-indacene-3-propionic acid (Invitrogen) to create N$^{ε}$-acetyl-Lys-tRNA$^{amb}$ ($ε$Ac-Lys-tRNA$^{amb}$) or N$^{ε}$-(BODIPY 576/589)-Lys-tRNA$^{amb}$ ($ε$BOP-Lys-tRNA$^{amb}$). These modified aa-tRNAs, purified by HPLC (Alder et al., 2008), were obtained from tRNA Probes, LLC.

### RTCs and RNCs for fluorescence experiments
In vitro translations (500 µl) to prepare RNCs contained 20 mM Hepes, pH 7.5; 2.8–3.5 mM (optimal concentration was determined experimentally for each lot and combination of macromolecular components) Mg(OAc)₂; 100–130 mM (optimized) KOAc, pH 7.5; 1 mM DTT; 0.2 mM spermidine; 8 µM S-adenosyl-methionine; 1x protease inhibitors (Erickson and Blobel, 1983); 0.2 U/µl RNasin (Promega); 40 µl of an energy-generating system containing 375 µM of each of the 20 amino acids except lysine, 120 mM creatine phosphate, and 0.12 U/µl\e creatine phosphokinase; 60–80 µl (optimized) wheat germ extract (Erickson and Blobel, 1983); 40 µl mRNA; and 300 pmol of each of two modified aa-tRNAs as detailed below (tRNA Probes, LLC). When RTCs (membrane-bound RNCs) were desired, 40 nM purified canine SRP and 80 eqs of canine salt-washed ER rough microsomes (tRNA Probes, LLC) were also added to the above translations. mRNAs were incubated at 65°C for 5 min and then quickly cooled on ice before addition to translations to minimize any inhibition by mRNA secondary structure. Before addition of mRNA and tRNA, translations were incubated at 26°C for 7 min to complete the translation of any residual endogenous mRNA fragments. After mRNA and tRNA addition, reactions were incubated at 26°C for another 30–35 min. When working with longer nascent chain lengths (171 amino acid residues and longer), the aa-tRNAs were added 5 min after the beginning of translation to reduce aa-tRNA deacylation before incorporation.

Four samples were always prepared in parallel that differed only in the identities of the modified aa-tRNAs added to a translation: D received $ε$NBD-[$^{14}$C]Lys-tRNA$^{Lys}$ and $ε$Ac-[$^{3}$H]Lys-tRNA$^{amb}$; DA received $ε$NBD-[$^{14}$C]Lys-tRNA$^{Lys}$ and $ε$BOP-[$^{3}$H]Lys-tRNA$^{amb}$; A received $ε$Ac-[$^{14}$C]Lys-tRNA$^{Lys}$ and $ε$BOP-[$^{3}$H]Lys-tRNA$^{amb}$; and B received $ε$Ac-[$^{14}$C]Lys-tRNA$^{Lys}$ and $ε$Ac-[$^{3}$H]Lys-tRNA$^{amb}$. RTCs were purified away from NBD not in RTCs by a high salt wash and then gel filtration. At the end of a translation, each sample was adjusted to 500 mM in KOAc and incubated on ice for 10 min. Each sample was then loaded onto a separate gel filtration column (Sepharose CL-2B, 0.7 cm I.D. x 50 cm; column resin must be replaced every 3–4 runs to avoid sample contamination by materials that adsorb to the resin) that had been preequilibrated in buffer A (50 mM Hepes, pH 7.5, 40 mM KOAc, pH 7.5, 5 mM Mg(OAc)₂) and then preloaded with 2 ml of buffer B (20 mM Hepes, pH 7.5, 500 mM KOAc, pH 7.5, 3.2 mM Mg(OAc)₂; Haigh and Johnson, 2002). After chromatography at a very slow rate (2–3 drops/min; 4°C) to ensure dissociation of noncovalently bound NBDs, the membrane-bound RNCs (= RTCs) eluted in the void volume, typically in 1.1 ml (two 550 µl fractions). Free RNC samples lacking microsomes were treated

the same way, except that no high-salt wash was done and Sepharose CL-6B (1.5 cm I.D. x 20 cm) was used instead of Sepharose CL-2B (microsomes elute in the void volume of Sepharose CL-2B columns, while free RNCs elute in the void volume of Sepharose CL-6B columns). After gel filtration, the light-scattering signals of the four parallel samples were measured using either $\lambda_{ex} = 405$ nm, $\lambda_{em} = 420$ nm, or $\lambda_{ex} = 468$ nm, $\lambda_{em} = 485$ nm (no significant difference was observed between these choices) and equalized by diluting the samples as necessary before initiating spectral measurements.

More than 50% of the $\varepsilon$NBD-Lys-tRNA$^{Lys}$ added to a wheat germ translation of preprolactin incorporated its amino acid into protein (Crowley et al., 1993). However, in the PMP FRET studies, only ~0.5% of the $\varepsilon$NBD-Lys added to the translation was recovered in the void-volume gel filtration fractions that contained the 2TM and 3TM nascent chains in microsome-bound RTCs due to a combination of effects: losses during purification; less efficient translation of the PMPs than of pPL; insertion of the $\varepsilon$NBD-Lys late in the nascent PMP sequence; and the requirement for $\varepsilon$BOP-Lys-tRNA$^{amb}$ to translate the amber stop codon instead of a termination factor. The latter two effects increased the loss of $\varepsilon$NBD-Lys-tRNA$^{Lys}$ due to deacylation, especially because the large size of the BOP dye slowed its rate of incorporation. The NBD concentration in the samples analyzed by FRET was 1–2 nM, whereas the acceptor concentration was three- to fourfold larger (residual Lys-tRNA$^{Lys}$ competition with $\varepsilon$NBD-Lys-tRNA$^{Lys}$ reduced the amount of NBD incorporated in nascent chains containing $\varepsilon$BOP-Lys; Krieg et al., 1989).

### Steady-state fluorescence

Steady-state measurements were made at 4°C in buffer A on a Spex Fluorolog 3–22 or SLM-8100 photon-counting spectrofluorimeter with a 450-W xenon lamp, two excitation monochromators, one (SLM) or two (Spex) emission monochromators, and a cooled low-background Hamamatsu R928 PMT. Samples were maintained at 4°C while nitrogen was flushed through the sample compartment to prevent condensation from forming on the 4 × 4-mm quartz microcuvettes. After additions to a sample, the solution was mixed thoroughly with a 2 × 2-mm magnetic stirring bar as described previously (Dell et al., 1990). Samples were then placed in the sample chamber for 5 min and allowed to equilibrate to 4°C before any measurements were made. To obtain an emission intensity measurement, five successive 5-second integrations of emission intensity were recorded and averaged.

### FRET

D, DA, A, and B samples that differ only in the number of fluorescent dyes (0, 1, or 2) in the nascent chain were prepared, purified, and examined in parallel to correct for background spectral signals. Aliquots (250 µl) of the purified and scattering-equalized D, DA, A, and B samples of RTCs or RNCs were placed into each of four cuvettes. The emission intensities (F) were measured at $\lambda_{ex} = 468$ nm, $\lambda_{em} = 530$ nm (4 nm bandpass) to focus on the donor dye emission. Because the signal recorded for the blank is due to light scattering and background fluorescence, and the signal from A is caused by light scattering, background fluorescence, and direct excitation of the acceptor (i.e., not emission due to FRET from the donor dye), the net emission intensities due to donor dye fluorescence in the D and DA samples, net $F_D$ and net $F_{DA}$, were determined by subtracting $F_B$ from $F_D$ and $F_A$ from $F_{DA}$.

To accurately compare net $F_{DA}$ with net $F_D$, the number of donor dyes in the D and DA samples had to be determined by quantifying the $\varepsilon$NBD-[$^{14}$C]Lys content in 200 µl of each sample (Crowley et al., 1993). The double-label counting efficiencies of the liquid scintillation counter were determined experimentally, using standard solutions of [$^3$H]H$_2$O and [$^{14}$C]glucose in the same scintillation cocktail system used for the samples, to be 0.60 and 0.16 for $^{14}$C, and 0.0 and 0.4 for $^3$H in the two windows. $F_D$ was then normalized to the same number of donor dyes as in $F_{DA}$. Because the NBD is too far from BOP to affect its absorbance, the FRET efficiency E is given by E = 1 – ($Q_{DA}/Q_D$) = 1 – (normalized net $F_{DA}$)/(normalized net $F_D$). E quantifies the acceptor-dependent quenching of donor emission intensity due to FRET. Although the average distance between the donor and acceptor dyes, R, can be calculated from E, the uncertainties associated with $\kappa^2$, the lengths of the probe-to-nascent chain tethers, and the dynamic equilibrium between nascent chain conformations (see Results) preclude a definitive determination of the actual polypeptide conformation. Thus, to monitor nascent chain folding, we have focused on changes in E, and hence R, as the nascent chain moves through the ribosomal tunnel.

### Determination of $R_0$

$R_0$, the distance between the donor and acceptor dyes at which FRET efficiency is 50%, was determined experimentally (Johnson et al., 1982) for

the NBD-BOP donor-acceptor pair in RTC complexes. $R_0^6 = (8.79 \times 10^{-5})QJ_{DA}n^{-4}\kappa^2$, where $R_0$ is in Å, Q is the quantum yield of the donor in the absence of the acceptor, $J_{DA}$ is the spectral overlap integral in M$^{-1}$cm$^{-1}$nm$^4$, n is the refractive index of the medium between donor and acceptor, and $\kappa^2$ is a geometric factor that depends on the relative orientation of the transition dipoles of the donor and acceptor dyes. The overlap of the corrected NBD emission spectrum and the BOP ($\varepsilon_{575}$ from 83,000 M$^{-1}$cm$^{-1}$) absorbance spectrum in 2TM$_{L12}$DA2 RTCs (Fig. 2 A) yielded a value of $4.7 \times 10^{15}$ M$^{-1}$cm$^{-1}$nm$^4$ for $J_{DA}$, and n was assumed to be 1.4 (Johnson et al., 1982).

The quantum yield of NBD in free $\varepsilon$NBD-Lys was determined experimentally (Mutucumarana et al., 1992) using disodium fluorescein in 0.1 M NaOH as the standard (Q = 0.92; Weber and Teale, 1957). The corrected emission intensities ($\lambda_{ex} = 468$ nm) were integrated from 500 to 625 nm, and the Q of $\varepsilon$NBD-Lys was found to be 0.04 in buffer A. The fluorescence lifetime of $\varepsilon$NBD-Lys was 1.3 ns in buffer A, but the average fluorescence lifetime, $<\tau>$, was much higher when the NBD was incorporated in or next to a nascent chain TMS and located in the ribosome tunnel (Table I; Lin et al., 2011). If one assumes that the NBD extinction coefficient is not significantly different for free $\varepsilon$NBD-Lys and $\varepsilon$NBD-Lys in an RTC-bound nascent chain, then Q is directly proportional to $\tau$. The average quantum yield of NBD in the ribosome tunnel is given by $Q_{NBD-RTC}/Q_{NBD-free} = \tau_{NBD-RTC}/\tau_{NBD-free} = Q_{NBD-RTC}/0.04 = 4.7–5.0/1.3$, and $Q_{NBD-RTC} = 0.15$.

Because $\kappa^2$ cannot be determined experimentally in a nonrigid system, $R_0$ is typically calculated by assuming that the orientations of the donor and acceptor transition dipoles are dynamically randomized during the excited-state lifetime of the donor dye. For such randomly oriented dyes, $\kappa^2 = 2/3$, and the resulting $R_0$ value is designated $R_0(2/3)$. Values for R calculated assuming $\kappa^2 = 2/3$ typically differ by less than 10% from those determined by crystallography when such comparisons can be made (e.g., Stryer, 1978; Wu and Brand, 1992; also compare tRNA-tRNA distance in solution by FRET [Johnson et al., 1982] and in a crystal structure [Yusupov et al., 2001]). The measured $R_0(2/3)$ for the NBD-BOP in the membrane-bound PMP RNCs was therefore 47 Å.

### $\kappa^2$ Uncertainty

The theoretical upper and lower limits of $\kappa^2$, and hence of $R_0$, can be determined from anisotropy (r) or polarization data that indicate the freedom of rotation of the dyes in the sample. The measured anisotropy values for the NBD and BOP dyes were the same for probes flanking TMS1, TMS2, and TMS3, and for all lengths of nascent chains in membrane-bound RNCs (Table II; Woolhead et al., 2004). Furthermore, the same anisotropies were observed after the full-length protein had been translated and released into the membrane bilayer. Because the anisotropy averaged 0.29 for NBD and 0.29 for BOP, each dye had significant freedom of rotation in our samples, and was not bound tightly to the ribosome. Furthermore, the similarity in the anisotropies inside and outside the ribosome tunnel indicate that the rotation of the large BOP dye was not detectably restricted by the spatial limitations of the eukaryotic ribosome tunnel, perhaps because the BOP is located at the end of a flexible lysine side chain. We observed the same phenomenon with BOF and BOP dyes flanking TMS1 (Woolhead et al., 2004).

The 0.29 anisotropies yield a maximum range of 0.10 to 3.25 for $\kappa^2$ in our samples (Dale et al., 1979). This corresponds to a $-27\%$ to $+30\%$ maximum uncertainty in $R_0$ due to orientation effects. However, as discussed previously (Johnson et al., 1982; Watson et al., 1995; Woolhead et al., 2004), the actual uncertainty is closer to 10%, largely because of the statistical improbability of some dye orientations (Hillel and Wu, 1976; Stryer, 1978; Wu and Brand, 1992) and the flexibility of the dye tethers (Wu and Brand, 1992).

### Time-resolved fluorescence

Fluorescence lifetimes were measured as detailed in Lin et al. (2011). The background phase and modulation data from a sample lacking NBD were subtracted from the corresponding data from an equivalent sample containing NBD that was prepared in parallel (Reinhart et al., 1991). Background-subtracted data from three or more independent experiments were combined and fit to several different models to determine which model provided the simplest fit while still yielding a low $\chi^2$ value using Vinci multidimensional fluorescence spectroscopy analysis software (ISS, Inc.). The best fit was almost always obtained by assuming two discrete exponential decay components. The fit of the data were not significantly improved by assuming the samples contained three components with distinguishable lifetimes, nor by using a Lorentzian fit instead of a discrete fit. The molar fraction of dyes with $\tau_n$ is given by $f_n$, from which the average lifetime, $<\tau>$, was calculated.

To examine the ribosome dependency of the observed lifetime, the NBD τ was measured for free $2TM_{L12}DA2_{130}$ RNCs in the absence of the acceptor dyes (Table I). The free RNCs were then treated with 2 mM puromycin (37°C, 30 min), followed by 5 mM EDTA (pH 7.5) and 20 µg/ml RNase A (final concentrations) at 37°C for 30 min to release the nascent chains from ribosomes. After measuring the NBD τ of this sample, proteinase K was added to 0.1 mg/ml and the sample was incubated at 37°C for 30 min to digest the nascent chain before measuring the NBD τ again.

### Photocrosslinking experiments

In vitro translations (50 µl) contained the above components with 30 pmol of εANB-[$^{14}$C]Lys-tRNA$^{Lys}$ (tRNA Probes, LLC), 50 µCi of [$^{35}$S]Met, an excess of the desired length of truncated mRNA containing a single Lys codon at the desired position, and glutathione instead of DTT. For RTCs, 40 nM SRP and 16 equivalents of column-washed microsomes (both from tRNA Probes, LLC) were also added. Samples were incubated at 26°C for 30 min in the dark and then photolyzed as before (McCormick et al., 2003). After photolysis, free RNCs or membrane-bound RTCs were centrifuged through a sucrose cushion buffer (130 µl; 0.5 M sucrose, 25 mM Hepes, pH 7.5, 120 mM KOAc, pH 7.5, 3 mM Mg(OAc)$_2$) in a TLA-100 rotor (Beckman Coulter; 100,000 rpm; 4°C; 3 min for RTCs or 10 min for free RNCs). Pellets destined for immunoprecipitation are discussed below; all other samples were resuspended in 50 µl of 50 mM Hepes, 5 mM EDTA at pH 7.5 and incubated with 1 µg of RNase A (26°C, 10 min) to remove residual peptidyl-tRNA before the addition of sample buffer and analysis by 10–15% SDS-PAGE as described previously (McCormick et al., 2003). Radioactive bands were visualized using a phosphorimager (model FX; Bio-Rad Laboratories).

### Immunoprecipitations

Pellets of photolyzed samples were resuspended in 50 µl of 3% (wt/vol) SDS, 50 mM Tris-HCl, pH 7.5, and incubated (55°C, 30 min) before the volume was adjusted to 500 µl with buffer B (150 mM NaCl, 50 mM Tris-HCl, pH 7.5, 1% [vol/vol] Triton X-100). The diluted samples were precleared by rocking with 30 µl of protein A–Sepharose at room temperature for 1 h before the Sepharose beads were removed by sedimentation. 4 µl of rabbit antiserum against the N terminus of L17 (Pool, 2009) were added to each supernatant, and the samples were rocked overnight at 4°C. After the addition of 40 µl of protein A–Sepharose, each sample was rocked for another 2 h at 4°C. The immunoprecipitated material was recovered by sedimentation, washed twice with buffer B, and once with buffer B lacking Triton X-100. After RNase treatment and SDS-PAGE as above, the radioactive immunoprecipitated material was visualized using a phosphorimager (model FX; Bio-Rad Laboratories).

### Online supplemental material

Figure S1 shows the VSVG, OP2, and OP3 TMS sequences and the probe locations at the TMSs. Online supplemental material is available at http://www.jcb.org/cgi/content/full/jcb.201103118/DC1.

## References

Alder, N.N., and A.E. Johnson. 2004. Cotranslational membrane protein biogenesis at the endoplasmic reticulum. *J. Biol. Chem.* 279:22787–22790. http://dx.doi.org/10.1074/jbc.R400002200

Alder, N.N., Y. Shen, J.L. Brodsky, L.M. Hendershot, and A.E. Johnson. 2005. The molecular mechanisms underlying BiP-mediated gating of the Sec61 translocon of the endoplasmic reticulum. *J. Cell Biol.* 168:389–399. http://dx.doi.org/10.1083/jcb.200409174

Alder, N.N., R.E. Jensen, and A.E. Johnson. 2008. Fluorescence mapping of mitochondrial TIM23 complex reveals a water-facing, substrate-interacting helix surface. *Cell.* 134:439–450. http://dx.doi.org/10.1016/j.cell.2008.06.007

Armache, J.-P., A. Jarasch, A.M. Anger, E. Villa, T. Becker, S. Bhushan, F. Jossinet, M. Habeck, G. Dindar, S. Franckenberg, et al. 2010a. Cryo-EM structure and rRNA model of a translating eukaryotic 80S ribosome at 5.5-A resolution. *Proc. Natl. Acad. Sci. USA.* 107:19748–19753. http://dx.doi.org/10.1073/pnas.1009999107

Armache, J.-P., A. Jarasch, A.M. Anger, E. Villa, T. Becker, S. Bhushan, F. Jossinet, M. Habeck, G. Dindar, J. Franckenberg, et al. 2010b. Localization of eukaryote-specific ribosomal proteins in a 5.5-Å cryo-EM map of the 80S eukaryotic ribosome. *Proc. Natl. Acad. Sci. USA.* 107:19754–19759. http://dx.doi.org/10.1073/pnas.1010005107

Ben-Shem, A., L. Jenner, G. Yusupova, and M. Yusupov. 2010. Crystal structure of the eukaryotic ribosome. *Science.* 330:1203–1209. http://dx.doi.org/10.1126/science.1194294

Berisio, R., F. Schluenzen, J. Harms, A. Bashan, T. Auerbach, D. Baram, and A. Yonath. 2003. Structural insight into the role of the ribosomal tunnel in cellular regulation. *Nat. Struct. Biol.* 10:366–370. http://dx.doi.org/10.1038/nsb915

Berndt, U., S. Oellerer, Y. Zhang, A.E. Johnson, and S. Rospert. 2009. A signal-anchor sequence stimulates signal recognition particle binding to ribosomes from inside the exit tunnel. *Proc. Natl. Acad. Sci. USA.* 106:1398–1403. http://dx.doi.org/10.1073/pnas.0808584106

Bhushan, S., M. Gartmann, M. Halic, J.-P. Armache, A. Jarasch, T. Mielke, O. Berninghausen, D.N. Wilson, and R. Beckmann. 2010a. alpha-Helical nascent polypeptide chains visualized within distinct regions of the ribosomal exit tunnel. *Nat. Struct. Mol. Biol.* 17:313–317. http://dx.doi.org/10.1038/nsmb.1756

Bhushan, S., H. Meyer, A.L. Starosta, T. Becker, T. Mielke, O. Berninghausen, M. Sattler, D.N. Wilson, and R. Beckmann. 2010b. Structural basis for translational stalling by human cytomegalovirus and fungal arginine attenuator peptide. *Mol. Cell.* 40:138–146. http://dx.doi.org/10.1016/j.molcel.2010.09.009

Bhushan, S., T. Hoffmann, B. Seidelt, J. Frauenfeld, T. Mielke, O. Berninghausen, D.N. Wilson, and R. Beckmann. 2011. SecM-stalled ribosomes adopt an altered geometry at the peptidyl transferase center. *PLoS Biol.* 9:e1000581–e1000581. http://dx.doi.org/10.1371/journal.pbio.1000581

Bornemann, T., J. Jöckel, M.V. Rodnina, and W. Wintermeyer. 2008. Signal sequence-independent membrane targeting of ribosomes containing short nascent peptides within the exit tunnel. *Nat. Struct. Mol. Biol.* 15:494–499. http://dx.doi.org/10.1038/nsmb.1402

Braakman, I., H. Hoover-Litty, K.R. Wagner, and A. Helenius. 1991. Folding of influenza hemagglutinin in the endoplasmic reticulum. *J. Cell Biol.* 114:401–411. http://dx.doi.org/10.1083/jcb.114.3.401

Cheng, Z., and R. Gilmore. 2006. Slow translocon gating causes cytosolic exposure of transmembrane and lumenal domains during membrane protein integration. *Nat. Struct. Mol. Biol.* 13:930–936. http://dx.doi.org/10.1038/nsmb1146

Choi, K.M., and R. Brimacombe. 1998. The path of the growing peptide chain through the 23S rRNA in the 50S ribosomal subunit; a comparative cross-linking study with three different peptide families. *Nucleic Acids Res.* 26:887–895. http://dx.doi.org/10.1093/nar/26.4.887

Choi, K.M., J.F. Atkins, R.F. Gesteland, and R. Brimacombe. 1998. Flexibility of the nascent polypeptide chain within the ribosome—contacts from the peptide N-terminus to a specific region of the 30S subunit. *Eur. J. Biochem.* 255:409–413. http://dx.doi.org/10.1046/j.1432-1327.1998.2550409.x

Crowley, K.S., G.D. Reinhart, and A.E. Johnson. 1993. The signal sequence moves through a ribosomal tunnel into a noncytoplasmic aqueous environment at the ER membrane early in translocation. *Cell.* 73:1101–1115. http://dx.doi.org/10.1016/0092-8674(93)90640-C

Crowley, K.S., S. Liao, V.E. Worrell, G.D. Reinhart, and A.E. Johnson. 1994. Secretory proteins move through the endoplasmic reticulum membrane via an aqueous, gated pore. *Cell.* 78:461–471. http://dx.doi.org/10.1016/0092-8674(94)90424-3

Cruz-Vera, L.R., M.S. Sachs, C.L. Squires, and C. Yanofsky. 2011. Nascent polypeptide sequences that influence ribosome function. *Curr. Opin. Microbiol.* 14:160–166. http://dx.doi.org/10.1016/j.mib.2011.01.011

Dale, R.E., J. Eisinger, and W.E. Blumberg. 1979. The orientational freedom of molecular probes. The orientation factor in intramolecular energy transfer. *Biophys. J.* 26:161–193. http://dx.doi.org/10.1016/S0006-3495(79)85243-1

Daniel, C.J., B. Conti, A.E. Johnson, and W.R. Skach. 2008. Control of translocation through the Sec61 translocon by nascent polypeptide structure within the ribosome. *J. Biol. Chem.* 283:20864–20873. http://dx.doi.org/10.1074/jbc.M803517200

Dell, V.A., D.L. Miller, and A.E. Johnson. 1990. Effects of nucleotide- and aurodox-induced changes in elongation factor Tu conformation upon its interactions with aminoacyl transfer RNA. A fluorescence study. *Biochemistry.* 29:1757–1763. http://dx.doi.org/10.1021/bi00459a014

Devaraneni, P., B.J. Conti, Y. Matsumura, Z. Yang, A.E. Johnson, and W.R. Skach. 2011. Stepwise insertion and inversion of a type II signal anchor

sequence in the ribosome-Sec61 translocon complex. *Cell*. 146:134–147. http://dx.doi.org/ doi:10.1016/j.cell.2011.06.004

Do, H., D. Falcone, J. Lin, D.W. Andrews, and A.E. Johnson. 1996. The co-translational integration of membrane proteins into the phospholipid bilayer is a multistep process. *Cell*. 85:369–378. http://dx.doi.org/10.1016/S0092-8674(00)81115-0

Erdmann, F., N. Schäuble, S. Lang, M. Jung, A. Honigmann, M. Ahmad, J. Dudek, J. Benedix, A. Harsman, A. Kopp, et al. 2011. Interaction of calmodulin with Sec61α limits Ca²⁺ leakage from the endoplasmic reticulum. *EMBO J*. 30:17–31. http://dx.doi.org/10.1038/emboj.2010.284

Erickson, A.H., and G. Blobel. 1983. Cell-free translation of messenger RNA in a wheat germ system. *Methods Enzymol*. 96:38–50. http://dx.doi.org/10.1016/S0076-6879(83)96007-X

Fang, P., C.C. Spevak, C. Wu, and M.S. Sachs. 2004. A nascent polypeptide domain that can regulate translation elongation. *Proc. Natl. Acad. Sci. USA*. 101:4059–4064. http://dx.doi.org/10.1073/pnas.0400554101

Flanagan, J.J., J.-C. Chen, Y. Miao, Y. Shao, J. Lin, P.E. Bock, and A.E. Johnson. 2003. Signal recognition particle binds to ribosome-bound signal sequences with fluorescence-detected subnanomolar affinity that does not diminish as the nascent chain lengthens. *J. Biol. Chem*. 278:18628–18637. http://dx.doi.org/10.1074/jbc.M300173200

Gilbert, R.J.C., P. Fucini, S. Connell, S.D. Fuller, K.H. Nierhaus, C.V. Robinson, C.M. Dobson, and D.I. Stuart. 2004. Three-dimensional structures of translating ribosomes by Cryo-EM. *Mol. Cell*. 14:57–66. http://dx.doi.org/10.1016/S1097-2765(04)00163-7

Gong, F., and C. Yanofsky. 2002. Instruction of translating ribosome by nascent peptide. *Science*. 297:1864–1867. http://dx.doi.org/10.1126/science.1073997

Haigh, N.G., and A.E. Johnson. 2002. A new role for BiP: Gating the aqueous ER translocon pore during membrane protein integration. *J. Cell Biol*. 156:261–270. http://dx.doi.org/10.1083/jcb.200110074

Hamman, B.D., J.-C. Chen, E.E. Johnson, and A.E. Johnson. 1997. The aqueous pore through the translocon has a diameter of 40-60 A during cotranslational protein translocation at the ER membrane. *Cell*. 89:535–544. http://dx.doi.org/10.1016/S0092-8674(00)80235-4

Hamman, B.D., L.M. Hendershot, and A.E. Johnson. 1998. BiP maintains the permeability barrier of the ER membrane by sealing the lumenal end of the translocon pore before and early in translocation. *Cell*. 92:747–758. http://dx.doi.org/10.1016/S0092-8674(00)81403-8

Hegde, R.S., S. Voigt, T.A. Rapoport, and V.R. Lingappa. 1998. TRAM regulates the exposure of nascent secretory proteins to the cytosol during translocation into the endoplasmic reticulum. *Cell*. 92:621–631. http://dx.doi.org/10.1016/S0092-8674(00)81130-7

Hillel, Z., and C.-W. Wu. 1976. Statistical interpretation of fluorescence energy transfer measurements in macromolecular systems. *Biochemistry*. 15:2105–2113. http://dx.doi.org/10.1021/bi00655a012

Houben, E.N.G., R. Zarivach, B. Oudega, and J. Luirink. 2005. Early encounters of a nascent membrane protein: specificity and timing of contacts inside and outside the ribosome. *J. Cell Biol*. 170:27–35. http://dx.doi.org/10.1083/jcb.200503035

Ito, K., S. Chiba, and K. Pogliano. 2010. Divergent stalling sequences sense and control cellular physiology. *Biochem. Biophys. Res. Commun*. 393:1–5. http://dx.doi.org/10.1016/j.bbrc.2010.01.073

Johnson, A.E. 2005a. The co-translational folding and interactions of nascent protein chains: a new approach using fluorescence resonance energy transfer. *FEBS Lett*. 579:916–920. http://dx.doi.org/10.1016/j.febslet.2004.11.046

Johnson, A.E. 2005b. Fluorescence approaches for determining protein conformations, interactions and mechanisms at membranes. *Traffic*. 6:1078–1092. http://dx.doi.org/10.1111/j.1600-0854.2005.00340.x

Johnson, A.E. 2009. The structural and functional coupling of two molecular machines, the ribosome and the translocon. *J. Cell Biol*. 185:765–767. http://dx.doi.org/10.1083/jcb.200902014

Johnson, A.E., W.R. Woodward, E. Herbert, and J.R. Menninger. 1976. Nepsilon-acetyllysine transfer ribonucleic acid: a biologically active analogue of aminoacyl transfer ribonucleic acids. *Biochemistry*. 15:569–575. http://dx.doi.org/10.1021/bi00648a018

Johnson, A.E., H.J. Adkins, E.A. Matthews, and C.R. Cantor. 1982. Distance moved by transfer RNA during translocation from the A site to the P site on the ribosome. *J. Mol. Biol*. 156:113–140. http://dx.doi.org/10.1016/0022-2836(82)90462-4

Johnson, A.E., S. Liao, J. Lin, B.D. Hamman, H. Do, A. Cowie, and D.W. Andrews. 1995. The environment of nascent secretory and membrane proteins at the ER membrane during translocation and integration. *Protein Kinesis: the dynamics of protein trafficking and stability*. Cold Spring Harb. Symp. Quant. Biol. 60:71–82.

Kosolapov, A., and C. Deutsch. 2009. Tertiary interactions within the ribosomal exit tunnel. *Nat. Struct. Mol. Biol*. 16:405–411. http://dx.doi.org/10.1038/nsmb.1571

Krieg, U.C., P. Walter, and A.E. Johnson. 1986. Photocrosslinking of the signal sequence of nascent preprolactin to the 54-kilodalton polypeptide of the signal recognition particle. *Proc. Natl. Acad. Sci. USA*. 83:8604–8608. http://dx.doi.org/10.1073/pnas.83.22.8604

Krieg, U.C., A.E. Johnson, and P. Walter. 1989. Protein translocation across the endoplasmic reticulum membrane: identification by photocrosslinking of a 39-kD integral membrane glycoprotein as part of a putative translocation tunnel. *J. Cell Biol*. 109:2033–2043. http://dx.doi.org/10.1083/jcb.109.5.2033

Liao, S., J. Lin, H. Do, and A.E. Johnson. 1997. Both lumenal and cytosolic gating of the aqueous ER translocon pore are regulated from inside the ribosome during membrane protein integration. *Cell*. 90:31–41. http://dx.doi.org/10.1016/S0092-8674(00)80311-6

Lin, P.-J., C.G. Jongsma, S. Liao, and A.E. Johnson. 2011. Transmembrane segments of nascent polytopic membrane proteins control cytosol/ER targeting during membrane integration. *J. Cell Biol*. 195:41–54.

Lu, J., and C. Deutsch. 2005a. Folding zones inside the ribosomal exit tunnel. *Nat. Struct. Mol. Biol*. 12:1123–1129. http://dx.doi.org/10.1038/nsmb1021

Lu, J., and C. Deutsch. 2005b. Secondary structure formation of a transmembrane segment in Kv channels. *Biochemistry*. 44:8230–8243. http://dx.doi.org/10.1021/bi050372q

Lu, J., W.R. Kobertz, and C. Deutsch. 2007. Mapping the electrostatic potential within the ribosomal exit tunnel. *J. Mol. Biol*. 371:1378–1391. http://dx.doi.org/10.1016/j.jmb.2007.06.038

Mariappan, M., X. Li, S. Stefanovic, A. Sharma, A. Mateja, R.J. Keenan, and R.S. Hegde. 2010. A ribosome-associating factor chaperones tail-anchored membrane proteins. *Nature*. 466:1120–1124. http://dx.doi.org/10.1038/nature09296

McCormick, P.J., Y. Miao, Y. Shao, J. Lin, and A.E. Johnson. 2003. Cotranslational protein integration into the ER membrane is mediated by the binding of nascent chains to translocon proteins. *Mol. Cell*. 12:329–341. http://dx.doi.org/10.1016/S1097-2765(03)00304-6

Mingarro, I., I. Nilsson, P. Whitley, and G. von Heijne. 2000. Different conformations of nascent polypeptides during translocation across the ER membrane. *BMC Cell Biol*. 1:3. http://dx.doi.org/10.1186/1471-2121-1-3

Mutucumarana, V.P., E.J. Duffy, P. Lollar, and A.E. Johnson. 1992. The active site of factor IXa is located far above the membrane surface and its conformation is altered upon association with factor VIIIa. A fluorescence study. *J. Biol. Chem*. 267:17012–17021.

Nakatogawa, H., and K. Ito. 2002. The ribosomal exit tunnel functions as a discriminating gate. *Cell*. 108:629–636. http://dx.doi.org/10.1016/S0092-8674(02)00649-9

Nissen, P., J. Hansen, N. Ban, P.B. Moore, and T.A. Steitz. 2000. The structural basis of ribosome activity in peptide bond synthesis. *Science*. 289:920–930. http://dx.doi.org/10.1126/science.289.5481.920

Peterson, J.H., C.A. Woolhead, and H.D. Bernstein. 2010. The conformation of a nascent polypeptide inside the ribosome tunnel affects protein targeting and protein folding. *Mol. Microbiol*. 78:203–217.

Plath, K., W. Mothes, B.M. Wilkinson, C.J. Stirling, and T.A. Rapoport. 1998. Signal sequence recognition in posttranslational protein transport across the yeast ER membrane. *Cell*. 94:795–807. http://dx.doi.org/10.1016/S0092-8674(00)81738-9

Pool, M.R. 2009. A trans-membrane segment inside the ribosome exit tunnel triggers RAMP4 recruitment to the Sec61p translocase. *J. Cell Biol*. 185:889–902. http://dx.doi.org/10.1083/jcb.200807066

Rapoport, T.A. 2007. Protein translocation across the eukaryotic endoplasmic reticulum and bacterial plasma membranes. *Nature*. 450:663–669. http://dx.doi.org/10.1038/nature06384

Reinhart, G.D., P. Marzola, D.M. Jameson, and E. Gratton. 1991. A method for on-line background subtraction in frequency domain fluorometry. *J. Fluoresc*. 1:153–162. http://dx.doi.org/10.1007/BF00865362

Saksena, S., M.D. Summers, J.K. Burks, A.E. Johnson, and S.C. Braunagel. 2006. Importin α-16: a translocon associated protein that may facilitate sorting of integral membrane proteins to the nuclear envelope. *Nat. Struct. Mol. Biol*. 13:500–508. http://dx.doi.org/10.1038/nsmb1098

Seidelt, B., C.A. Innis, D.N. Wilson, M. Gartmann, J.-P. Armache, E. Villa, L.G. Trabuco, T. Becker, T. Mielke, K. Schulten, et al. 2009. Structural insight into nascent polypeptide chain-mediated translational stalling. *Science*. 326:1412–1415. http://dx.doi.org/10.1126/science.1177662

Skach, W.R. 2009. Cellular mechanisms of membrane protein folding. *Nat. Struct. Mol. Biol*. 16:606–612. http://dx.doi.org/10.1038/nsmb.1600

Stade, K., N. Jünke, and R. Brimacombe. 1995. Mapping the path of the nascent peptide chain through the 23S RNA in the 50S ribosomal subunit. *Nucleic Acids Res*. 23:2371–2380. http://dx.doi.org/10.1093/nar/23.13.2371

Stryer, L. 1978. Fluorescence energy transfer as a spectroscopic ruler. *Annu. Rev. Biochem*. 47:819–846. http://dx.doi.org/10.1146/annurev.bi.47.070178.004131

Teilum, K., J.C. Hoch, V. Goffin, S. Kinet, J.A. Martial, and B.B. Kragelund. 2005. Solution structure of human prolactin. *J. Mol. Biol.* 351:810–823. http://dx.doi.org/10.1016/j.jmb.2005.06.042

Tu, L.W., and C. Deutsch. 2010. A folding zone in the ribosomal exit tunnel for Kv1.3 helix formation. *J. Mol. Biol.* 396:1346–1360. http://dx.doi .org/10.1016/j.jmb.2009.12.059

Ujvári, A., R. Aron, T. Eisenhaure, E. Cheng, H.A. Parag, Y. Smicun, R. Halaban, and D.N. Hebert. 2001. Translation rate of human tyrosinase determines its *N*-linked glycosylation level. *J. Biol. Chem.* 276:5924–5931. http:// dx.doi.org/10.1074/jbc.M009203200

Vázquez-Laslop, N., H. Ramu, D. Klepacki, K. Kannan, and A.S. Mankin. 2010. The key function of a conserved and modified rRNA residue in the ribo-somal response to the nascent peptide. *EMBO J.* 29:3108–3117. http:// dx.doi.org/10.1038/emboj.2010.180

Watson, B.S., T.L. Hazlett, J.F. Eccleston, C. Davis, D.M. Jameson, and A.E. Johnson. 1995. Macromolecular arrangement in the aminoacyl-tRNA. elongation factor Tu.GTP ternary complex. A fluorescence energy transfer study. *Biochemistry*. 34:7904–7912. http://dx.doi.org/10.1021/ bi00024a015

Weber, G., and F.W.J. Teale. 1957. Determination of the absolute quantum yield of fluorescent solutions. *Trans. Faraday Soc.* 53:646–655. http://dx.doi. org/10.1039/tf9575300646

Wilson, D.N., and R. Beckmann. 2011. The ribosomal tunnel as a functional environment for nascent polypeptide folding and translational stalling. *Curr. Opin. Struct. Biol.* 21:274–282. http://dx.doi.org/10.1016/j.sbi .2011.01.007

Woolhead, C.A., P.J. McCormick, and A.E. Johnson. 2004. Nascent membrane and secretory proteins differ in FRET-detected folding far inside the ribosome and in their exposure to ribosomal proteins. *Cell*. 116:725–736. http://dx.doi.org/10.1016/S0092-8674(04)00169-2

Woolhead, C.A., A.E. Johnson, and H.D. Bernstein. 2006. Translation arrest requires two-way communication between a nascent polypeptide and the ribosome. *Mol. Cell*. 22:587–598. http://dx.doi.org/10.1016/j.molcel .2006.05.021

Wu, P., and L. Brand. 1992. Orientation factor in steady-state and time-resolved resonance energy transfer measurements. *Biochemistry*. 31:7939–7947. http://dx.doi.org/10.1021/bi00149a027

Yusupov, M.M., G.Z. Yusupova, A. Baucom, K. Lieberman, T.N. Earnest, J.H.D. Cate, and H.F. Noller. 2001. Crystal structure of the ribosome at 5.5 A resolution. *Science*. 292:883–896. http://dx.doi.org/10.1126/ science.1060089

Ziv, G., G. Haran, and D. Thirumalai. 2005. Ribosome exit tunnel can entropi-cally stabilize α-helices. *Proc. Natl. Acad. Sci. USA*. 102:18956–18961. http://dx.doi.org/10.1073/pnas.0508234102